Spring 2020

A broad Iceland plume associated with two phase transitions at the 660 km discontinuity: Constraints from receiver functions

Dan Wang

Department: Geosciences and Geological and Petroleum Engineering

A BROAD ICELAND PLUME ASSOCIATED WITH TWO PHASE TRANSITIONS AT THE 660 KM DISCONTINUITY: CONSTRAINTS FROM RECEIVER FUNCTIONS

by

DAN WANG

A DISSERTATION

Presented to the Graduate Faculty of the

MISSOURI UNIVERSITY OF SCIENCE AND TECHNOLOGY

In Partial Fulfillment of the Requirements for the Degree

DOCTOR OF PHILOSOPHY

in

GEOLOGY AND GEOPHYSICS

2020

Approved by:

Stephen S. Gao, Advisor
Kelly H. Liu
J. David Rogers
David Wronkiewicz
Youqiang Yu

PUBLICATION DISSERTATION OPTION

This dissertation consists of the following article that has been formatted in the style used by the Missouri University of Science and Technology:

Pages 3– 55, has been submitted to *Nature Communications.*

ABSTRACT

In spite of the fact that Iceland is frequently regarded as the archetypal example of mantle plumes, the existence, depth extent, origin, dimension and excess temperature of the hypothesized plume remain enigmatic and hotly debated. The controversy mostly originates from the limited vertical resolution of seismic tomography techniques and the associated uncertainty in the depth and lateral extents of the lower wavespeed anomaly. Here we utilize a robust receiver-function-based technique to image the topography of the 410 and 660 km discontinuities bordering the mantle transition zone beneath Iceland and surrounding oceanic regions, and construct thermal and seismic wavespeed models of the upper mantle and mantle transition zone based on the observations. The preferred model invokes a broad plume laterally extending ~1000 km originated from the lower mantle. The dominant phase transition across the 660-km discontinuity is the post-spinel transition in the peripheral area, but becomes the post-garnet transition in the central portion of the plume stem due to the excessive temperature anomaly. This phase transition variation significantly enlarges the plume dimension and enhances upwelling of plume material.

ACKNOWLEDGMENTS

I would like to express my appreciation and gratitude to my advisor, Dr. Stephen S. Gao, and to Dr. Kelly H. Liu for their outstanding and patient mentorship and guidance thoughout my Ph.D. study here at Missouri S&T. They are always encouraging, helping, and caring me no matter what kind of difficulties I encounter. They teach me not only how to be a good researcher, but also how to become a tough and optimistic person. Their advice and suggestions will provide lifelong benefits for me.

I am especially grateful to my dissertation committee: Dr. David Wronkiewicz, Dr. J. David Rogers, and Dr. Youqiang Yu. Dr. David Wronkiewicz provided a lot of suggestions and information from geochemistry and mineralogy aspects which leads to the comprehensive interpretation of my final paper. Dr. J. David Rogers always teaches me how to survive in the academia world in the future by providing his insights and experience thoughtout his career. He helps me a lot on my career development. Dr. Youqinag Yu provides a lot of insights and suggestions on my final models of my research paper. He always helps me anytime I have questions.

I would like to thank all my colleagues in the geophysics group at Missouri S&T for their help and support.

Finally, yet importantly, I would like to give my deep appreciation to my parents in China. Without your support and unconditional love, I would not have all the achievements I have today.

TABLE OF CONTENTS

Page

LIST OF ILLUSTRATIONS

PAPER I Page

NOMENCLATURE

Symbol	Description
γ	The relationship between P and S wavespeeds express as dln(Vs)/d ln(Vp)
Δ	The epicentral distance ranging from 30^o to 100^o

1. INTRODUCTION

Hotspot is the surface expression of perceived mantle plumes underneath. As a candidate for hotspot associated with the proposed plume, Iceland has been studies through years to solve the questions regarding to the mantle plume. The drifting of the North American and Eurasian plates causes continental breakup and large amounts of magma erupted during a short geological time at about 55-60 million years ago[1,2]. The excess amount of volcanism has been linked to the interaction between the Atlantic Mid-oceanic ridge and the Iceland hotspot[2]. However, mostly due to the anomalously large size of the surface uplift (Figures 1-2) relative to other perceived hotspots and a lack of an age-progressive volcanic track caused by the movement of the plate over a stationary mantle plume[2], the existence of a mantle plume beneath the region remains enigmatic. Seismic tomographic studies show that there is a strong low-velocity zone (LVZ) beneath Iceland and surrounding areas (Figures 1 - 3), indicating the existence of structures with hot temperature[3]. However, the depth extent of the LVZ remains ambiguous. Many regional tomography studies suggest that the LVZ is mostly confined in the upper mantle[4–7], probably due to the small aperture of seismic arrays in the study area[8] and the limited vertical resolution of the tomography techniques that is insufficient to reliably resolve the LVZ below the upper mantle[9]. Most global tomography studies, however, show a continuous LVZ down to the lower mantle which is consistent with a lower-mantle origin of the LVZ[10–13]. In particular, a recent global tomography study[13] suggests the existence of a broad plume (approximately 800-1000 km in diameter which is several times greater than the diameter of a typical plume) originating from the northern tip of

the African large low shear velocity provinces at the base of the lower mantle. A geodynamic modeling study indicates that such a broad mantle plume can be developed when there are two mineral phase transitions at the 660-km discontinuities, from ringwoodite to perovskite and from majorite garnet to perovskite[14], but observational evidence for the presence of the two phase transitions beneath Iceland is still lacking.

Here we utilize a receiver-function-based technique to image the 410 and 660 km discontinuities (d410 and d660, respectively) beneath Iceland to investigate the thermal state and the nature of phase transitions associated with the MTZ. The d410 has a positive Clapeyron slope[15] ranging from 1.5 to 3.0 MPa/K and represents the exothermic transition from olivine to wadsleyite, and the phase transition and the sign of the Clapeyron slope at the d660 are temperature-dependent. When the ambient temperature is less than 1800℃, the dominant phase transition is from ringwoodite to perovskite (which is termed post-spinel or pSp) with a Clapeyron slope ranging from -4.0 to -1.0 MPa/K (refs.15,16). At higher temperatures, the dominant phase transition is from majorite garnet to perovskite (post-garnet or pGt), which has a positive Clapeyron slope of +1.3 MPa/K (ref. 17). Previous receiver function studies to image the mantle transition zone beneath Iceland lead to contradictory conclusions regarding the vertical and lateral extents of the proposed Iceland plume[18–21].

PAPER

I. A BROAD ICELAND PLUME ASSOCIATED WITH TWO PHASE TRANSITIONS AT THE 660 KM DISCONTINUITY

ABSTRACT

In spite of the fact that Iceland is frequently regarded as the archetypal example of mantle plumes, the existence, depth extent, origin, dimension and excess temperature of the hypothesized plume remain enigmatic and hotly debated. The controversy mostly originates from the limited vertical resolution of seismic tomography techniques and the associated uncertainty in the depth and lateral extents of the lower wavespeed anomaly. Here we utilize a robust receiver-function-based technique to image the topography of the 410 and 660 km discontinuities bordering the mantle transition zone beneath Iceland and surrounding oceanic regions, and construct thermal and seismic wavespeed models of the upper mantle and mantle transition zone based on the observations. The preferred model invokes a broad plume laterally extending ~1000 km originated from the lower mantle. The dominant phase transition across the 660-km discontinuity is the post-spinel transition in the peripheral area, but becomes the post-garnet transition in the central portion of the plume stem due to the excessive temperature anomaly. This phase transition variation significantly enlarges the plume dimension and enhances upwelling of plume material.

1. INTRODUCTION

The drifting of the North American and Eurasian plates causes continental breakup and large amounts of magma erupted during a short geological time at about 55-60 million years ago[1,2]. The excess amount of volcanism has been linked to the interaction between the Atlantic Mid-oceanic ridge and the Iceland hotspot[2]. However, mostly due to the anomalously large size of the surface uplift (Figures 1-2) relative to other perceived hotspots and a lack of an age-progressive volcanic track caused by the movement of the plate over a stationary mantle plume[2], the existence of a mantle plume beneath the region remains enigmatic. Seismic tomographic studies show that there is a strong low-velocity zone (LVZ) beneath Iceland and surrounding areas (Figures 1-3), indicating the existence of structures with hot temperature[3]. However, the depth extent of the LVZ remains ambiguous. Many regional tomography studies suggest that the LVZ is mostly confined in the upper mantle[4–7], probably due to the small aperture of seismic arrays in the study area[8] and the limited vertical resolution of the tomography techniques that is insufficient to reliably resolve the LVZ below the upper mantle[9]. Most global tomography studies, however, show a continuous LVZ down to the lower mantle which is consistent with a lower-mantle origin of the LVZ[10–13]. In particular, a recent global tomography study[13] suggests the existence of a broad plume (approximately 800-1000 km in diameter which is several times greater than the diameter of a typical plume) originating from the northern tip of the African large low shear velocity provinces at the base of the lower mantle. A geodynamic modeling study indicates that such a broad mantle plume can be developed when there are two mineral phase transitions at the 660-

km discontinuities, from ringwoodite to perovskite and from majorite garnet to perovskite[14], but observational evidence for the presence of the two phase transitions beneath Iceland is still lacking.

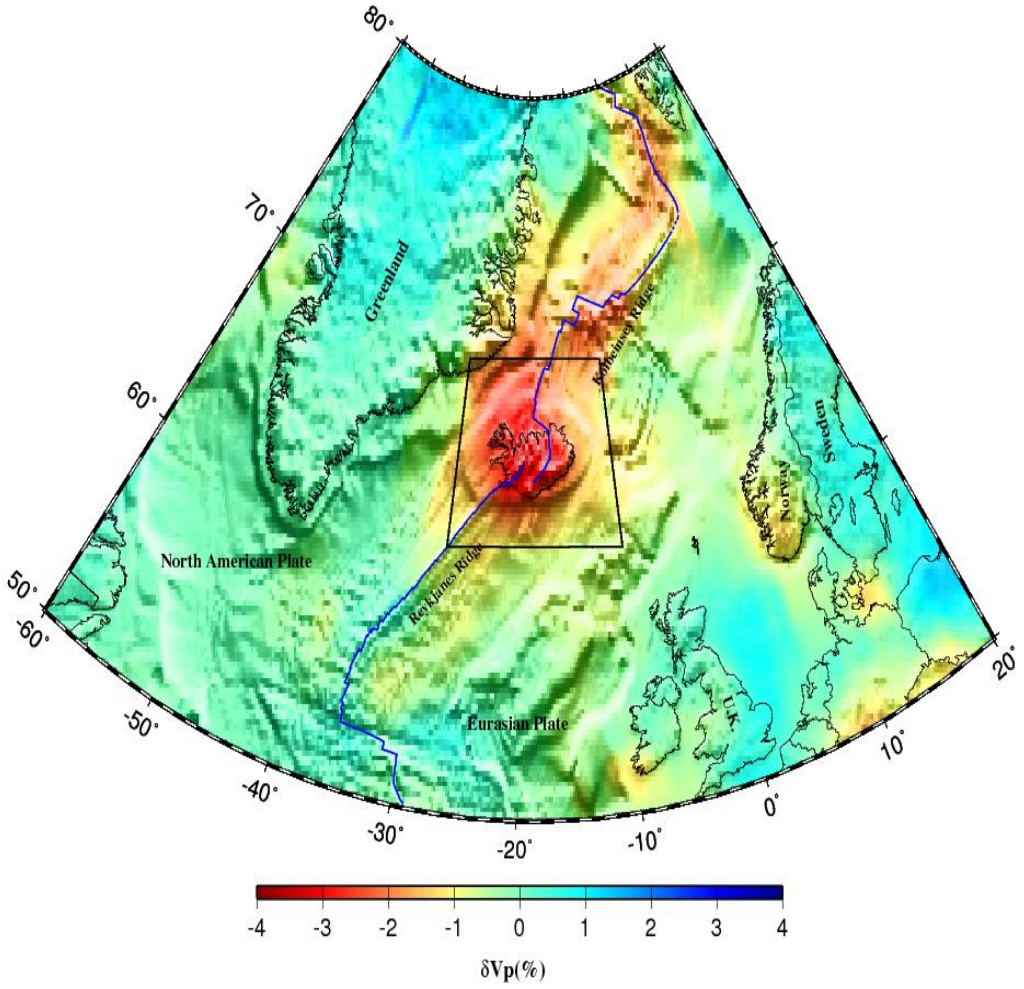

Figure 1. Average P wavespeed anomalies[24] in the upper mantle (0-410 km), showing a broad distribution of low Vp anomalies around the Iceland area.

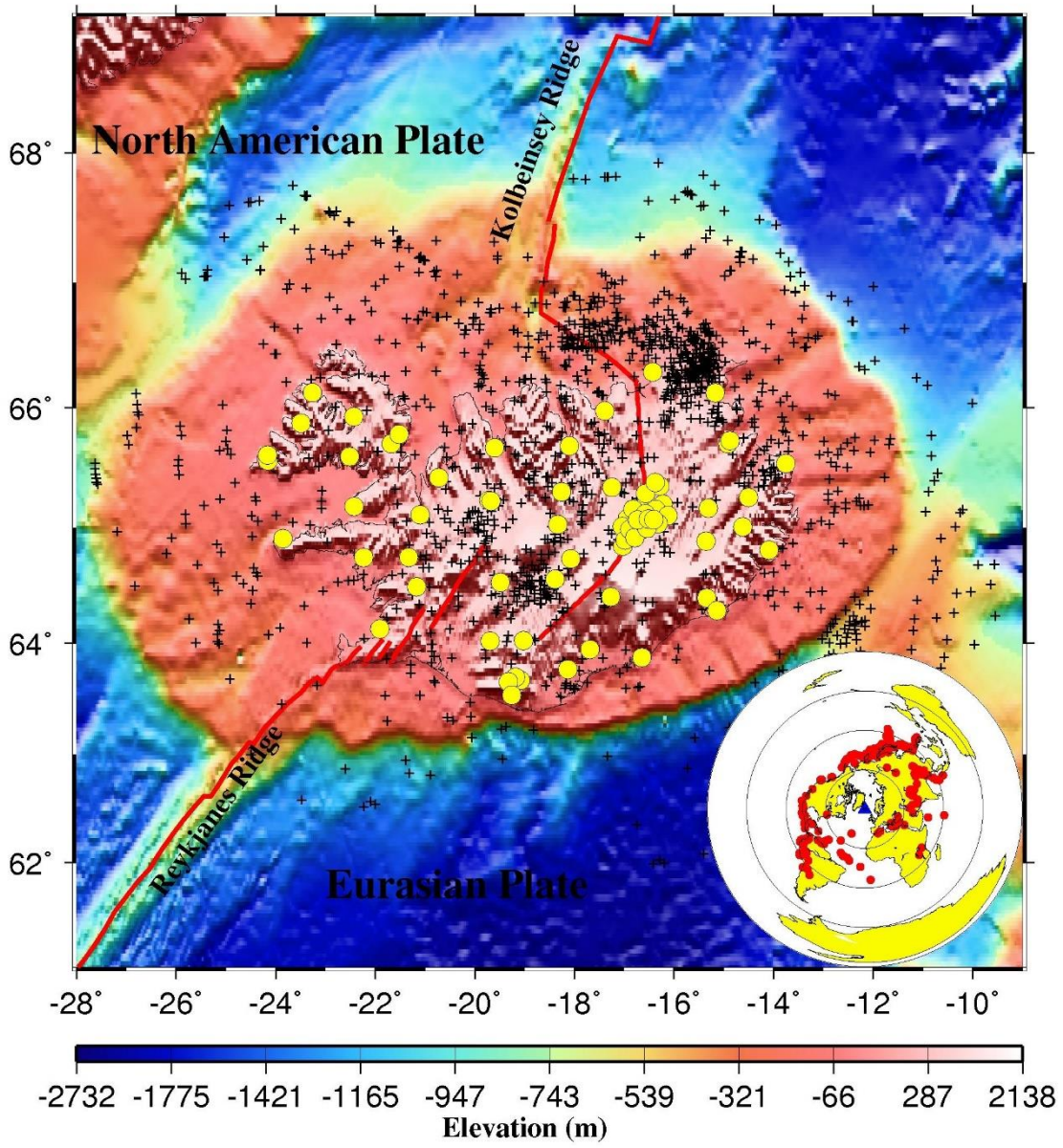

Figure 2. A topographic relief map of the study area showing seismic stations (yellow circles) used in this study, and the ray-piecing points (black pluses) at 535-km depth. The blue line indicates the mid-Atlantic ridge and the red triangles represent major volcanoes. The inset shows the event locations used in this study. The increment of the circles is 45˚ in epicentral distance.

Here we utilize a receiver-function-based technique to image the 410 and 660 km discontinuities (d410 and d660, respectively) beneath Iceland to investigate the thermal state and the nature of phase transitions associated with the MTZ. The d410 has a positive Clapeyron slope[15] ranging from 1.5 to 3.0 MPa/K and represents the exothermic transition from olivine to wadsleyite, and the phase transition and the sign of the Clapeyron slope at the d660 are temperature-dependent. When the ambient temperature is less than 1800℃, the dominant phase transition is from ringwoodite to perovskite (which is termed post-spinel or pSp) with a Clapeyron slope ranging from -4.0 to -1.0 MPa/K (refs.15,16). At higher temperatures, the dominant phase transition is from majorite garnet to perovskite (post-garnet or pGt), which has a positive Clapeyron slope of +1.3 MPa/K (ref. 17). Previous receiver function studies to image the mantle transition zone beneath Iceland lead to contradictory conclusions regarding the vertical and lateral extents of the proposed Iceland plume[18–21].

2. RECEIVER FUNCTION STACKING RESULTS

The procedure that we used for the acquisition and processing of the seismic data from a total of 87 seismic stations (Figures 1-2) as well as the method of stacking the receiver functions under the non-plane wave assumption can be found in the Method section. As demonstrated in Figure 3 and Supplementary Figures S1 and S2, robust arrivals corresponding to the 410 and d660 can be unambiguously identified on the vast majority of the resulting depth series. Because the 1-D IASP91 Earth model was used for time-depth conversion, the resulting depths and MTZ thickness (Figure 4-7 and

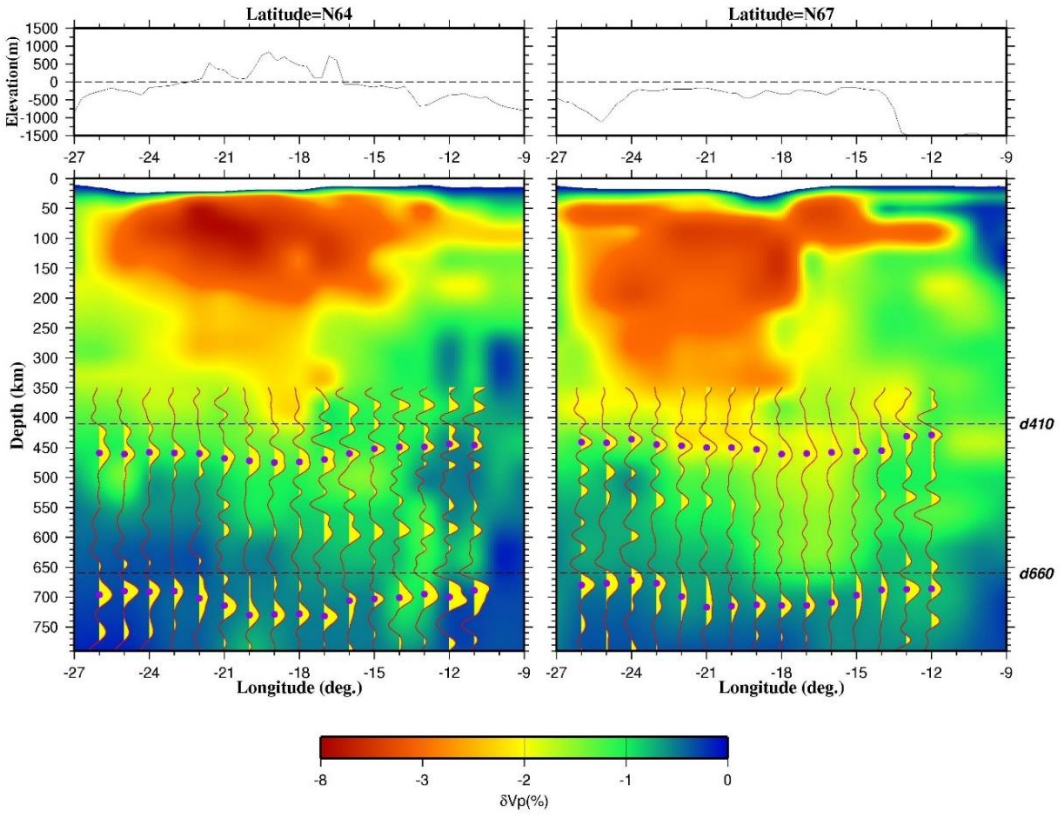

Figure 3. Example stacked and time-depth converted receiver functions along two E-W profiles. The background image shows Vp anomalies[24], and the purple dots on the traces indicate the picked arrivals for the d410 and d660. The upper panels show the elevation change along these profiles. Note that the entire mapped region is characterized by negative Vp anomalies for both profiles.

Supplementary Table S1) are apparent rather than true values. The apparent depths of the d410 and d660 in all the circular bins (with averages of 451±13 km and 701±16 km, respectively) are greater than the global averages of 410 and 660 km and are positively correlated, with a correlation coefficient of 0.83, suggesting the presence of upper mantle LVZ that affects the apparent depths of both discontinuities. We also attempted to obtained the true depths by correcting the apparent depths using several velocity models (refs. 22–24), but found large inconsistences in the corrected discontinuity depths among

the velocity models (Supplementary Figures S3-S5). However, the MTZ thickness pattern, from which the main conclusions are drawn, remains similar regardless of the choice of models. Therefore, we will interpret the results primarily based on the variations of the apparent discontinuity depths and MTZ thickness, with references to the corrected depths.

The largest d410 and d660 apparent depths (483 km and 737 km respectively) are located beneath south-central Iceland, which is close to the previously proposed center of the Iceland mantle plume[19]. The average MTZ thickness is 249±9 km, which is within the range of estimated global MTZ thickness of 242.0 -250.8 km[25,26]. A NE-SW elongated zone in central Iceland is characterized by apparently deeper d410 and d660 discontinuities comparing to the surrounding area, with a normal to slightly thicker MTZ (Figures 4-7). The average apparent depth in this zone (which is termed "central zone") for the d410 and d660 and the MTZ thickness is 456±15 km, 712± 15 km, and 256±6 km, respectively. The slightly greater-than-normal MTZ thickness is due to the larger depression of the d660 relative to that of the d410. Outside the central zone, which is referred as the peripheral area, both the d410 and d660 are apparently shallower than those in the central zone, with apparent depths of d410 and d660 as 447±9 km and 689±9 km respectively and an MTZ thickness of 242±8 km. The thinning of the MTZ is caused by the smaller apparent depression of the d660 relative to that of the d410.

We next explore a number of models separately for the central zone and peripheral area based on the observed MTZ thickness and discontinuity depths, by considering two major factors affecting the apparent depths of the d410 and d660: 1) velocity anomalies in the upper mantle and MTZ relative to the IASP91 standard earth

model; and 2) temperature anomalies in the vicinity of the MTZ discontinuities estimated from the P wave velocity anomalies using a scaling factor of δVp/ δT = 0.00048 km s -1 /°C (ref. 27) and a Clapeyron slope of +2.9 MPa/K for the d410 (ref. 15).

3. MODEL FOR THE PERIPHERAL AREA

The simplest model that can explain the apparent depression of the MTZ discontinuities and thickening of the MTZ for the peripheral area involves a Vp anomaly of -0.95% traversing from the lower mantle to the surface (Supplementary Figure S10a). The required Vp anomaly is comparable to that estimated using seismic tomography (Supplementary Figure S11-S18), and the associated temperature anomaly of the LVZ is about +178 K calculated based on the scaling factor[27], leading to an uplift of 6 km of the d660 (Supplementary Figure S10a) calculated using a Clapeyron slope of -1.3 MPa K^{-1} (ref. [20]). Assuming a normal temperature of 1600 ^{o}C at the d660 (ref. [28]), the estimated temperature at the d660 is 1778 °C which is lower than the 1800 ^{o}C needed for the post-garnet phase transition to become dominant[29]. Therefore, the post-spinel transition dominates in this area. The low velocities in both the upper mantle and MTZ lead to an apparent depression of 35 km of the d660, and thus the net apparent d660 depression is 29 km, which is comparable to the observed value in this area. If other Clapeyron slopes [15,29,30] (e.g., -2.1 MPa/K, -1 MPa/K, -2.5 MPa/K) are used for the d660, the predicted d660 depths are still close to the observed values, with differences ranging from -6 km to +1 km from the observed value. Therefore, observations in the peripheral area can be explained by a thermal upwelling with a temperature anomaly of about 178 ^{o}C

originating from the lower mantle and traversing the MTZ and the upper mantle (Supplementary Figure S10a).

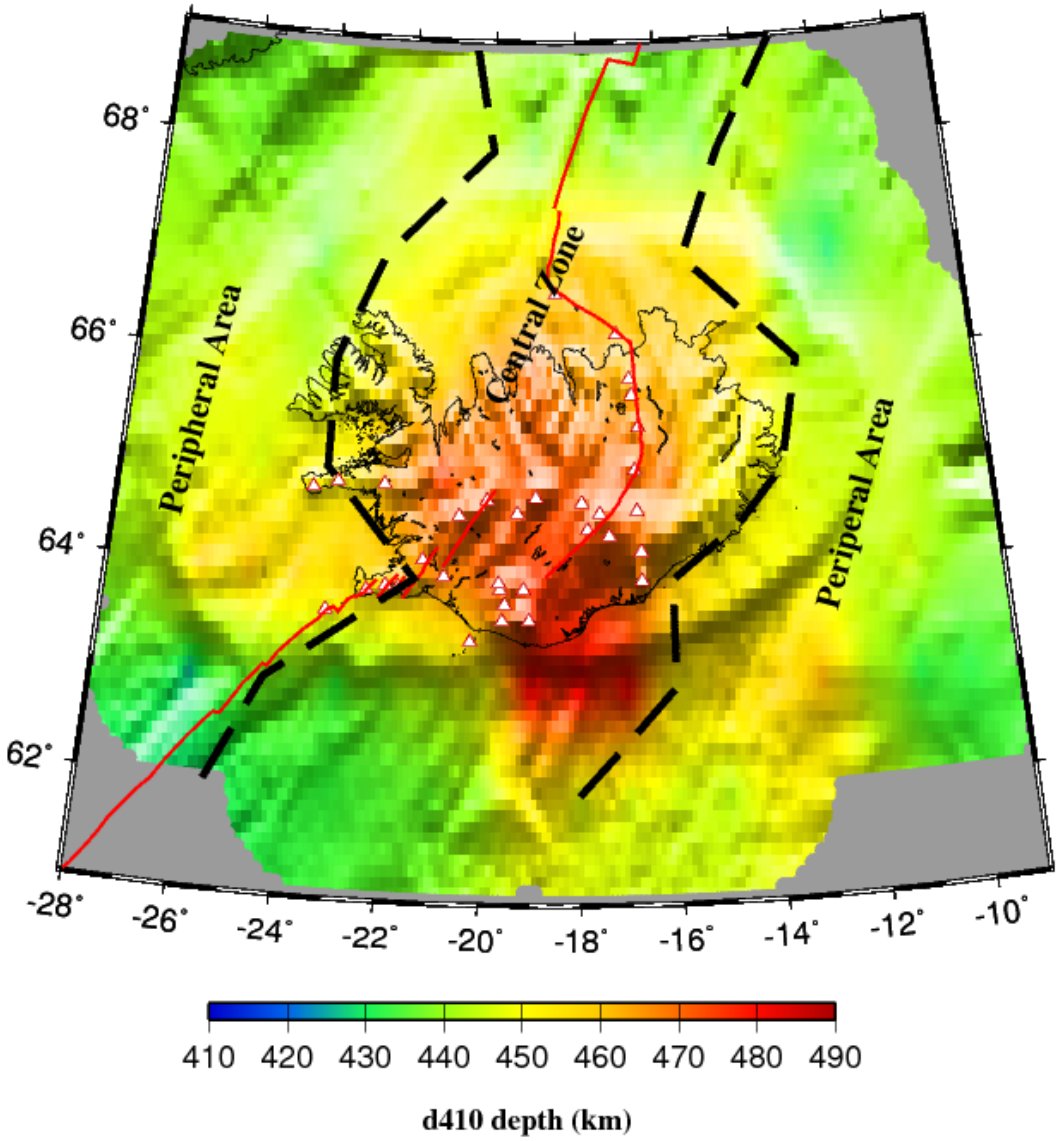

Figure 4. Resulting apparent depths of the apparent d410 depth. The red line indicates the plate boundary and the white triangles represent the distribution of major volcanoes. The black dashed lines represent the boundary of the peripheral area and central zone divided based on the MTZ thickness variations.

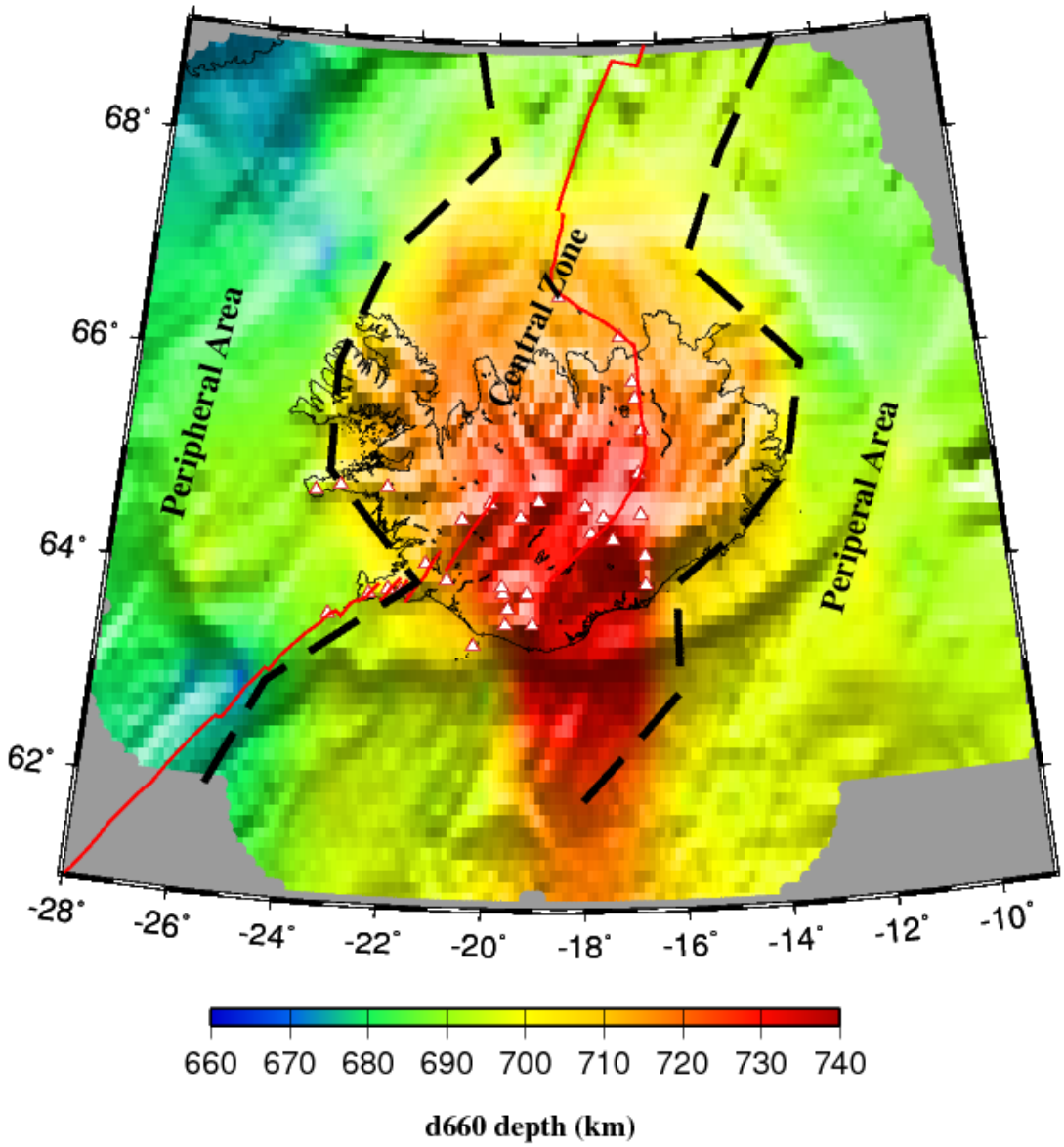

Figure 5. Resulting apparent depths of the apparent d660 depth. The red line indicates the plate boundary and the white triangles represent the distribution of major volcanoes. The black dashed lines represent the boundary of the peripheral area and central zone divided based on the MTZ thickness variations.

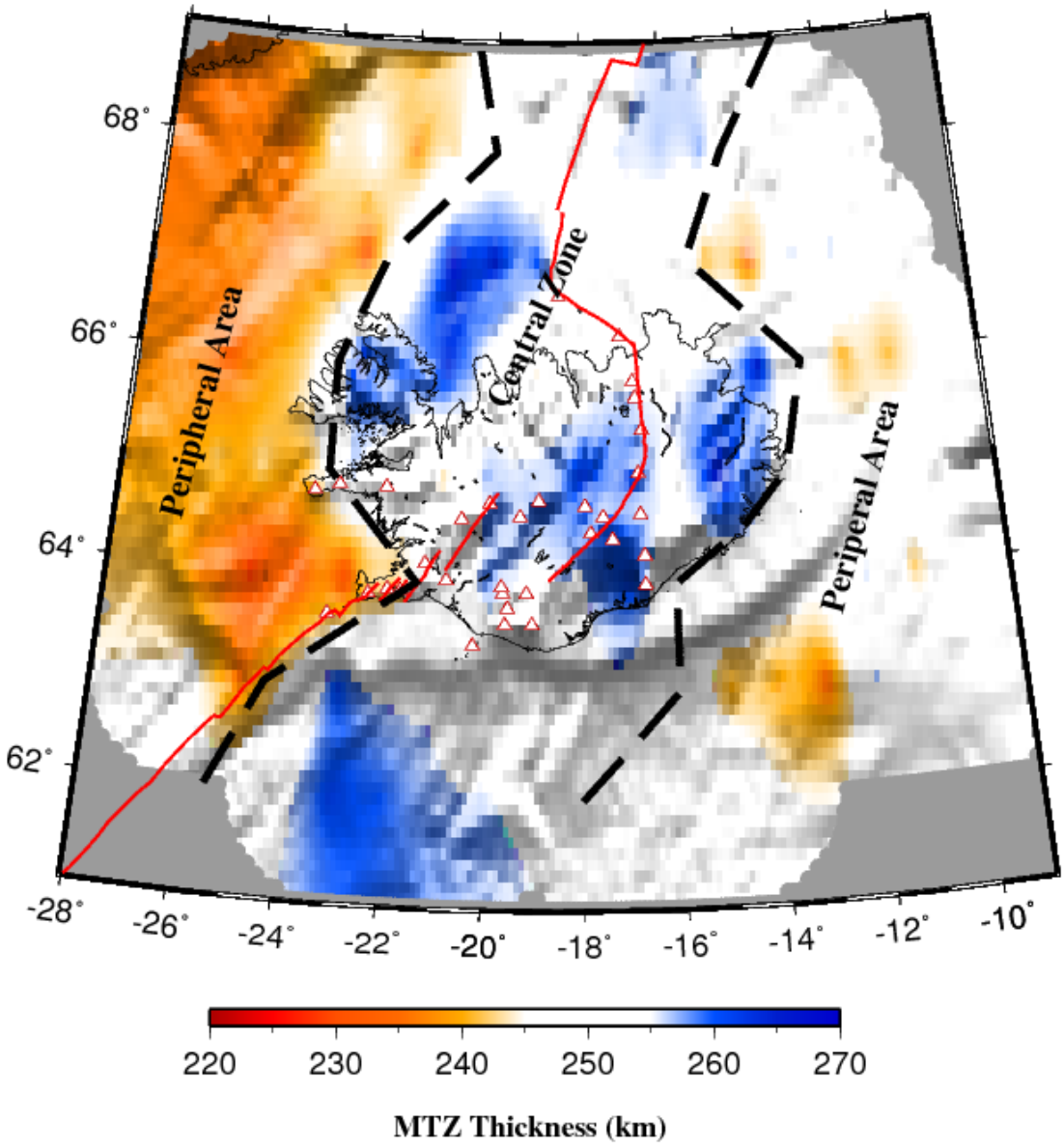

Figure 6. Resulting spatial distribution of the MTZ thickness. The red line indicates the plate boundary and the white triangles represent the distribution of major volcanoes. The black dashed lines represent the boundary of the peripheral area and central zone divided based on the MTZ thickness variations.

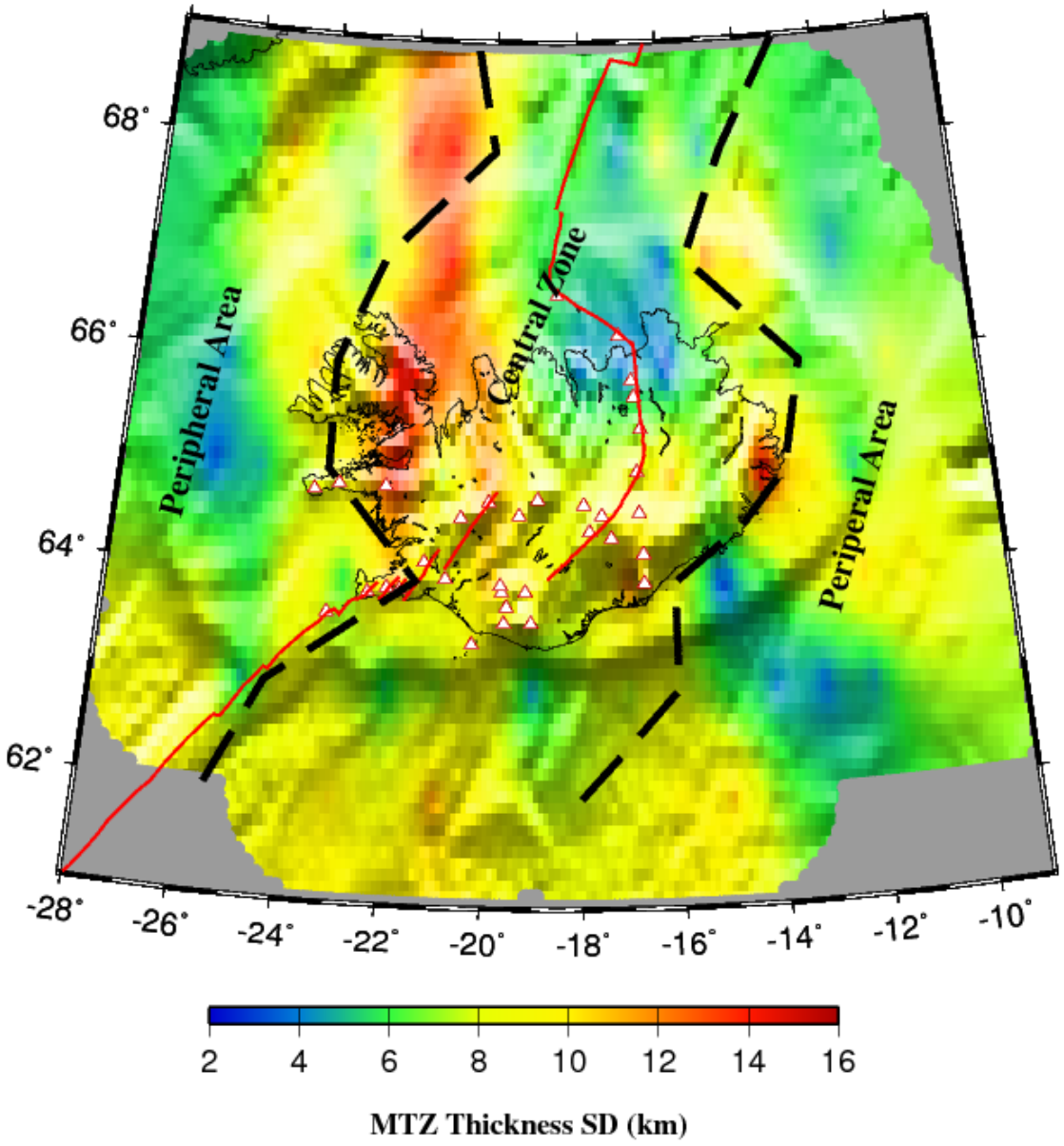

Figure 7. Resulting spatial distribution of the MTZ thickness standard deviation (SD). The red line indicates the plate boundary and the white triangles represent the distribution of major volcanoes. The black dashed lines represent the boundary of the peripheral area and central zone divided based on the MTZ thickness variations.

4. MODELS FOR THE CENTRAL ZONE

Because the central zone has an MTZ thickness of 256±6 km which is close to the global average of 250 km (Figures 4-7 and Supplementary Figures S3-S9), an LVZ limited in the upper mantle (Supplementary Figure S10b) with a Vp anomaly of -1.92% could in principle account for the observations. However, this model cannot explain the significant low velocities in the MTZ found by most seismic tomography studies (Supplementary Figures S11-S18). If the LVZ extends to the lower mantle and the d660 represents the post-spinel transition (Supplementary Figure S10c), the required Vp anomaly is -1.16%, and the resulting total depression by combining the effects of velocity and thermal (218 K, calculated using the scaling factor27) anomalies for the d410 and d660 is 46 and 35 km, respectively, leading to an MTZ that is 11 km thinner than the global average which is inconsistent with the slightly thicker than normal MTZ observed in this area. If we assume that the dominant phase transition is post-garnet, on the other hand, the depression for the d660 becomes 51 km (calculated using a Clapeyron slope of +1.3 MPa/K, ref. 17) which results in a slight MTZ thickening of 5 km which is in agreement with the observations (Supplementary Figure S10d). The assumption that the dominant phase transition across the d660 is the post-garnet phase transition, which dominates in temperatures higher than 1800℃ (ref. 17,29), is consistent with the estimated temperature in the MTZ (~1818 ^{o}C).

5. IMPLICATIONS FOR MANTLE PLUME DYNAMICS

A recent geodynamic modeling study[14] suggests that when both the post-spinel and post-garnet phase transitions are involved at the d660, an upwelling plume experiences significant increases in the size, strength of upwelling, and the volume flux relative to typical mantle plumes with relatively lower temperature. The enhancement of penetration capability and volume flux is mostly caused by the decomposition of ringwoodite into garnet and magnesiowüstite and the associated density drop [14,29]. Our results provide strong observational evidence for such a model. Additionally, the required critical temperature for the change of dominant phase transition to occur[14] is comparable to the estimated temperature in the central zone.

Increasing temperature toward the plume center results in a change of dominant phase transition across the d660 from post-spinel in the peripheral area to post-garnet in the central zone (Figure 4). The co-existence of the two phase transitions explains the abnormally large lateral plume dimension, which is larger than the area sampled by the receiver functions (Supplementary Figure S19) and could reach ~1000 km on the basis of seismic tomography images (Supplementary Figures S11-18). The anomalously large size of the surface uplift and the excessive volcanism observed in Iceland and the surrounding Atlantic region can be attributed to the broad mantle plume confirmed by the study.

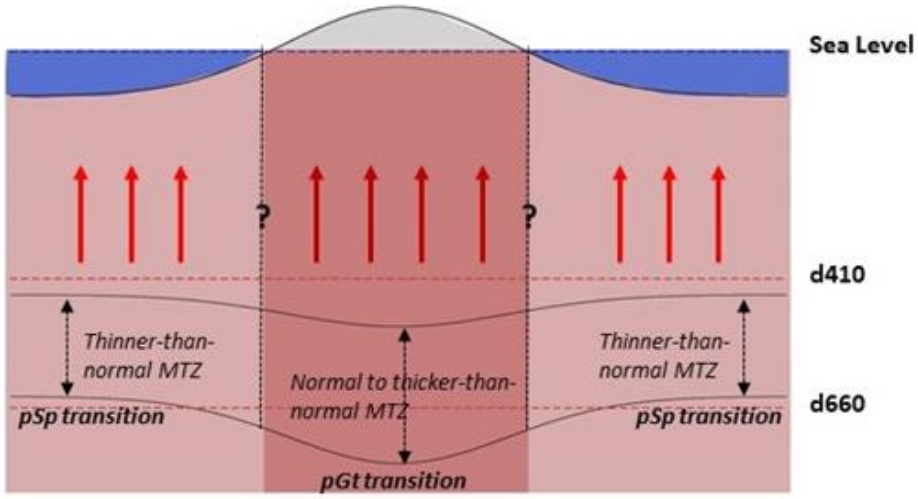

Figure 8. A schematic E-W cross-section showing the major characteristics of the topography of the MTZ discontinuities. The dominant mineral phase transition across the d660 is post-spinel (pSp) beneath the peripheral area and post-garnet (pGt) in the central zone due to the increasing temperature toward the proposed plume center. The red arrows indicate thermal upwelling.

6. METHODS

The data requesting and processing procedure used in this study is the same as that used in ref. [31] for a MTZ study in the contiguous United States, and is briefly summarized here. The cut-off magnitude for the events used to request data is calculated by $Mc= 5.2 + (\Delta- \Delta min)/180.0- \Delta min) – D/Dmax$, where Δ is the epicentral distance ranging from 30^o to 100^o, $\Delta min=30^o$ is the minimum epicentral distance, D is the focal depth in km, and Dmax=700 km. A four-pole, two–pass Bessel filter is applied to the original data, and seismograms with a first arrival signal-to-noise ratio of 4.0 on the vertical component are rejected. A total of 1399 high-quality receiver functions are

obtained using the water-level deconvolution procedure in the frequency domain[32]. Additionally, we apply a set of exponential weighting functions to reduce the effects of the degenerating PP arrivals[33].

We image the d410 and d660 discontinuities using the same method in ref. [31]. Under the non-plane wave assumption, we apply the normal moveout corrections based on the IASP91 standard earth model and compute the geographic coordinates of the ray piercing points at a depth of 535 km for each of the RFs (Figures 1-2). Then we stack the RFs in the consecutive circles of 1^{o} radius. The number of RFs per circle is shown in Supplementary Figure S19. A bootstrap resampling procedure[34] with 50 iterations is used to calculate the mean and standard deviation of the d410 and d660 depths, and the MTZ thickness by picking the maximum stacking amplitude in a preset depth window of 380-440 km for the d410 and 650-710 km for the d660. We apply a visual checking of the stacked traces to reject unreliable peaks with small peak amplitudes and multiple peaks with similar amplitudes by adjusting the searching window to pick the discontinuity depth with respect to the largest amplitude of the arrivals.

6.1. VELOCITY CORRECTIONS USING DIFFERENT GLOBAL VELOCITY MODELS

Since the resolution of regional velocity models is very low below 400 km depth due to the limited aperture of seismic arrays at Iceland[8], global models are used to perform velocity corrections. Three different global velocity models are used: TX2019[22], GAP2013[23], and UU2007[24]. Among these velocity models, TX2019 contains both Vp and Vs models, and others are P-wave models. For TX2019, we perform the correction

using both the Vp and Vs models and with the Vp model with different γ factors (1.8-3.0) which is expressed as dln(Vs)/d ln(Vp). For other models, a constant γ factor of 2.0 is used. The resulting corrected depths and MTZ thickness are shown in Supplementary Figures S3-S9. By comparing the results, we conclude that the corrected depths of both discontinuities are significantly different when different models and different choices of γ factor are used, but the MTZ thickness pattern remains similar. Therefore, we interpret the results based on the variations of the apparent discontinuity depths and MTZ thickness obtained from the IASP91 standard earth model.

ACKNOWLEDGEMENTS

Data used in the study were obtained from the Data Management Center of the Incorporated Research Institutions for Seismology, and from the Observatories and Research Facilities for European Seismology. The study was partially supported by the U.S. National Science Foundation Award No. 1919789.

COMPETING INTERESTS

The authors declare no competing interests.

AUTHOR CONTRIBUTIONS

D.W. and S.G. conceived the paper. D.W. wrote the paper with help from S.G. and K.L. S.G. and K.L. developed the computing codes used in the study.

SUPPLEMENTARY INFORMATION

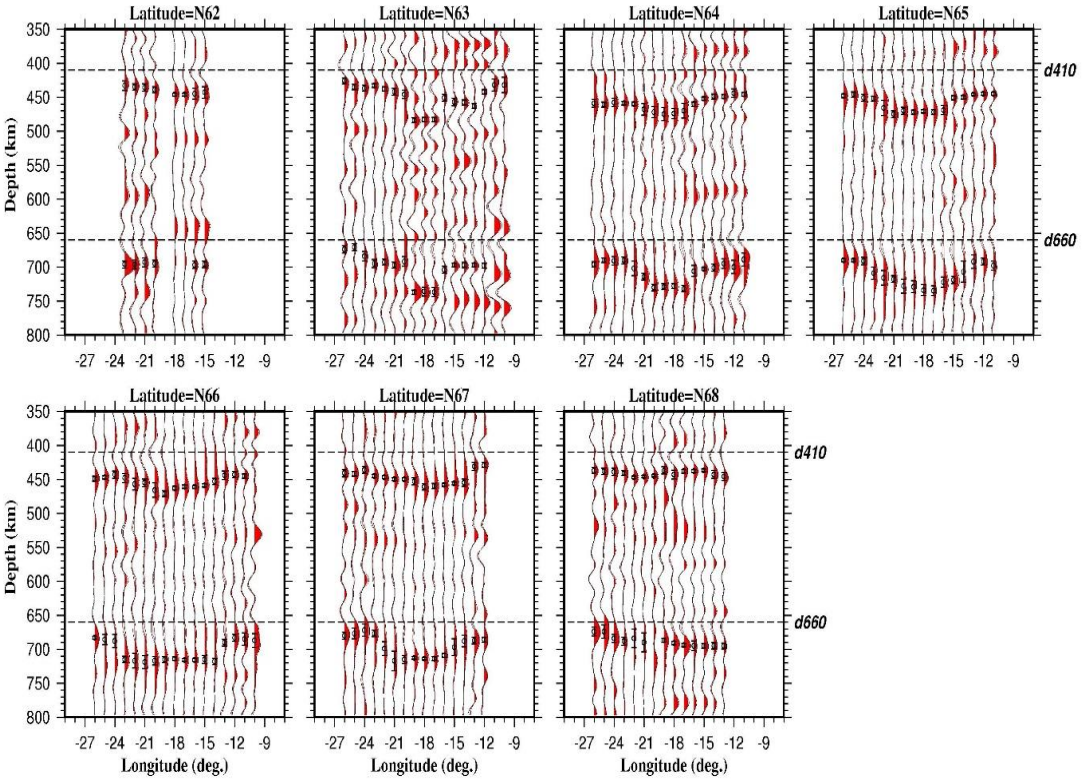

Figure S1. Resulting stacked receiver functions along all the 7 latitudinal profiles. The circles and error bars represent the picked discontinuity arrivals and the standard deviations of the MTZ discontinuities depths, respectively.

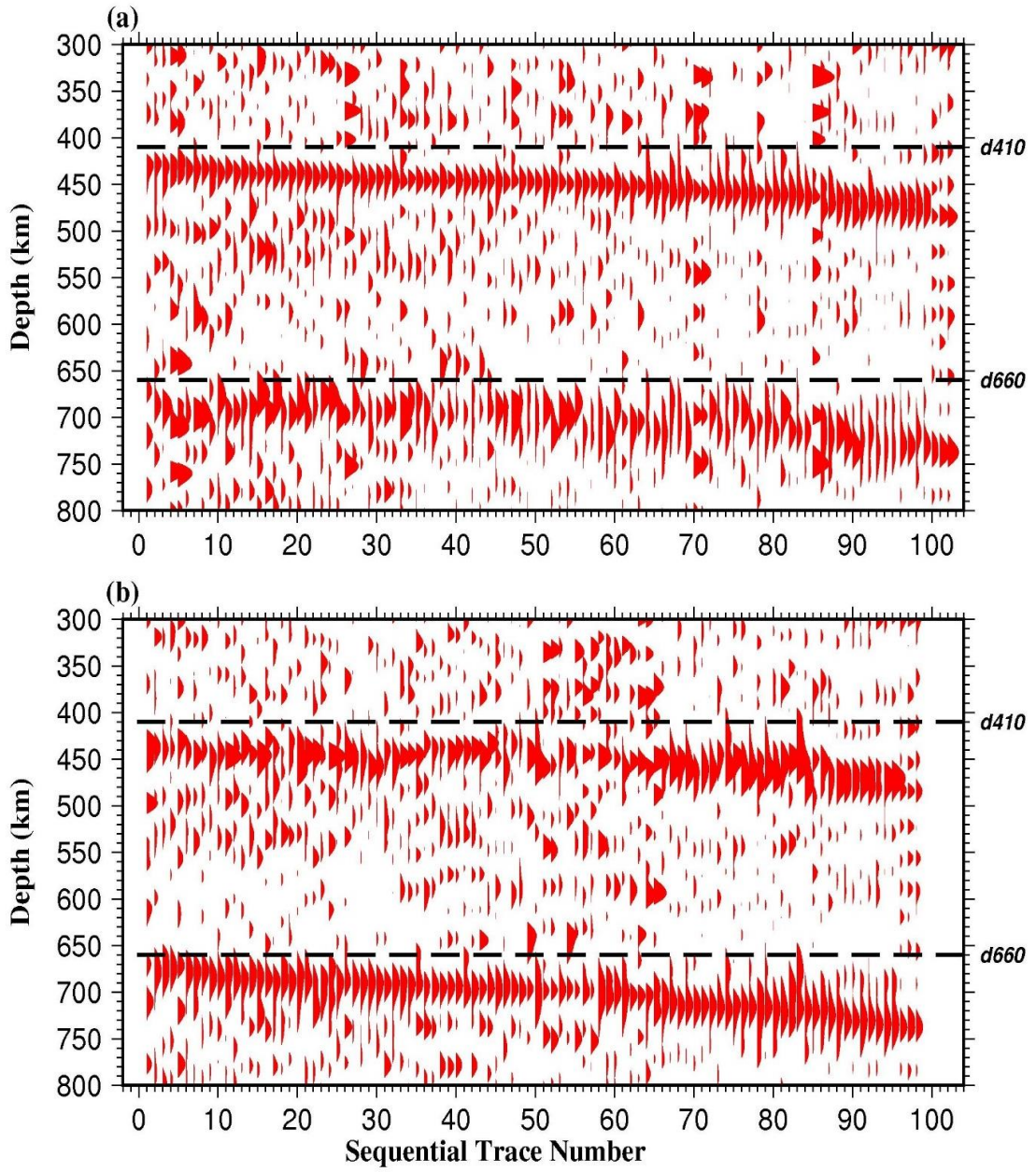

Figure S2. Traces for each bin with 1˚ degree radius plotting with sequentially increasing depth of **(a)** d410 **(b)** d660. Clear P-to-S arrivals can be observed at 102 bins for the d410, 98 bins for the d660, and 97 bins for both.

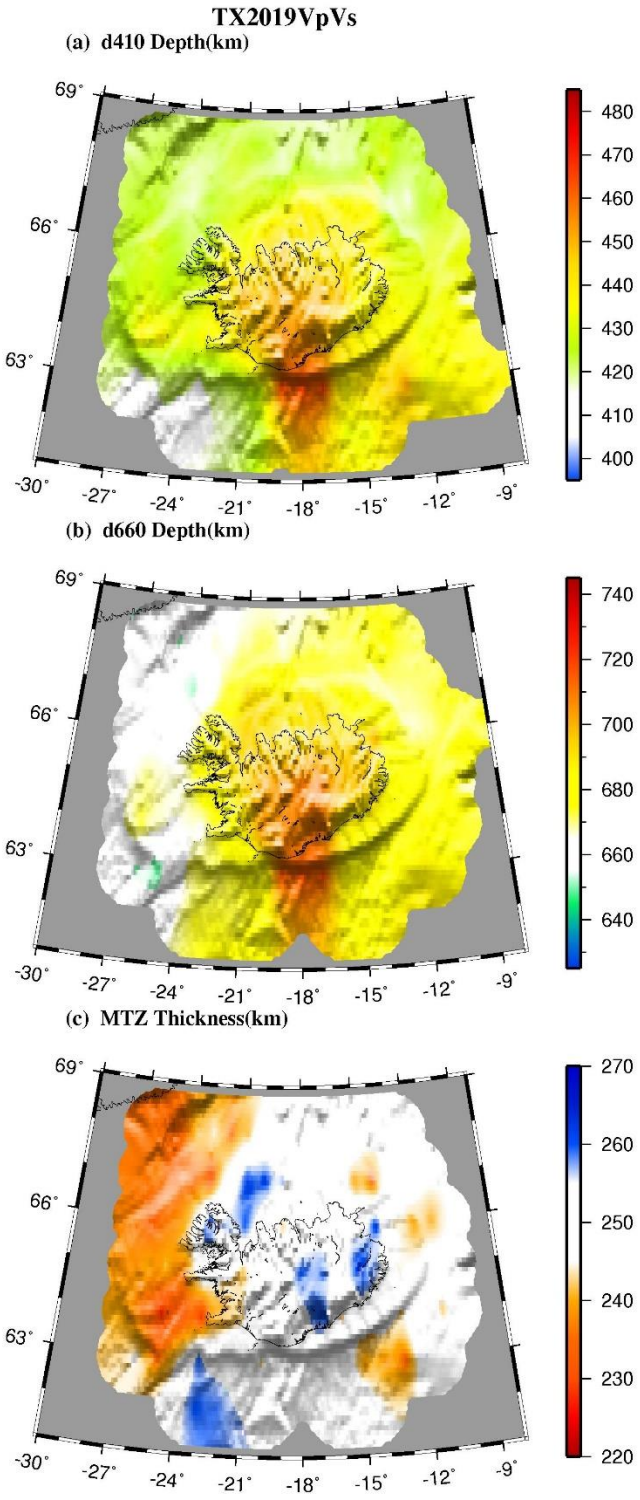

Figure S3. Wavespeed-corrected results using the TX2019 Vp and Vs models.

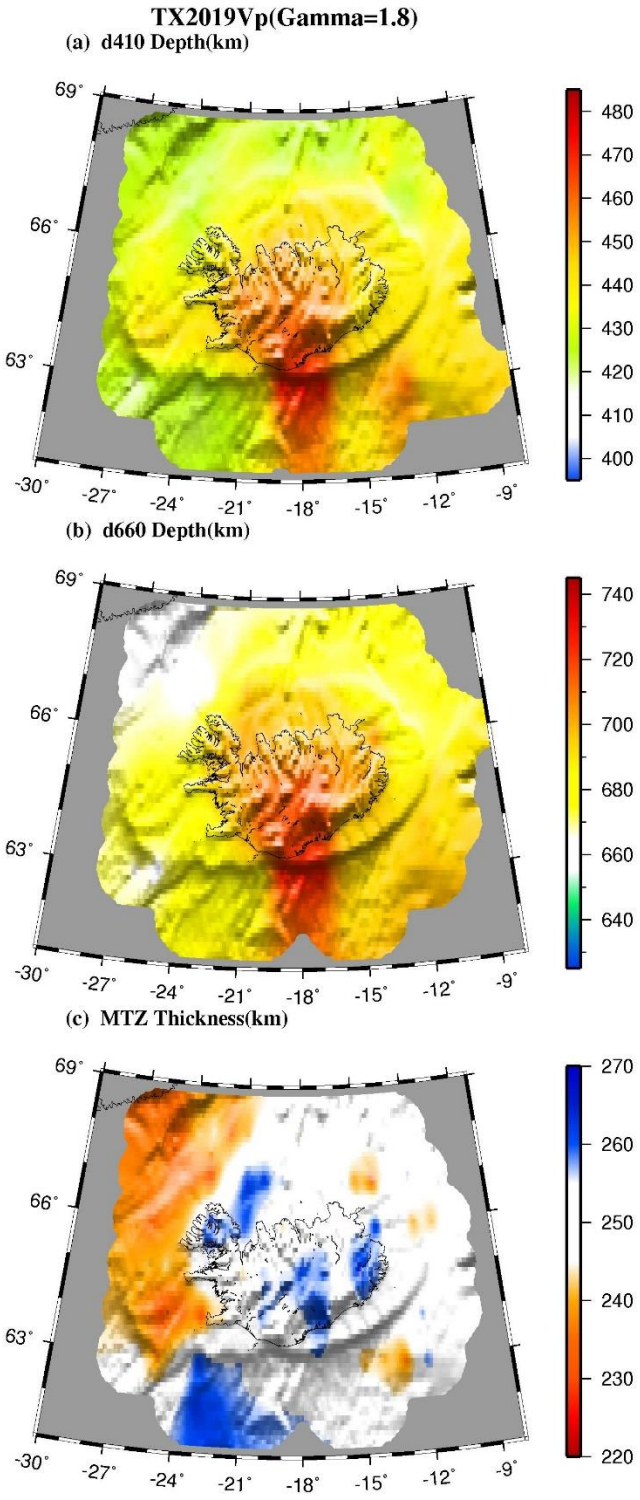

Figure S4. Correction results using the TX2019 Vp model with γ factors of 1.8.

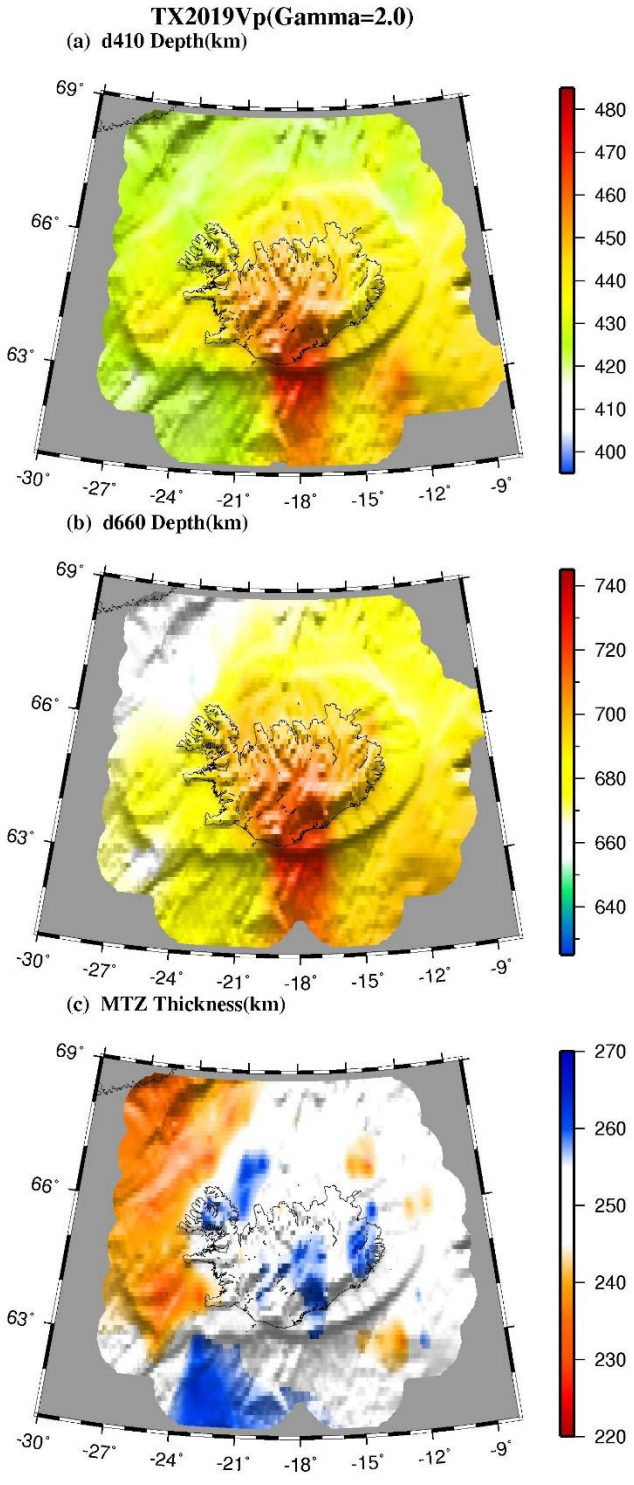

Figure S5. Correction results using the TX2019 Vp model with γ factors of 2.0.

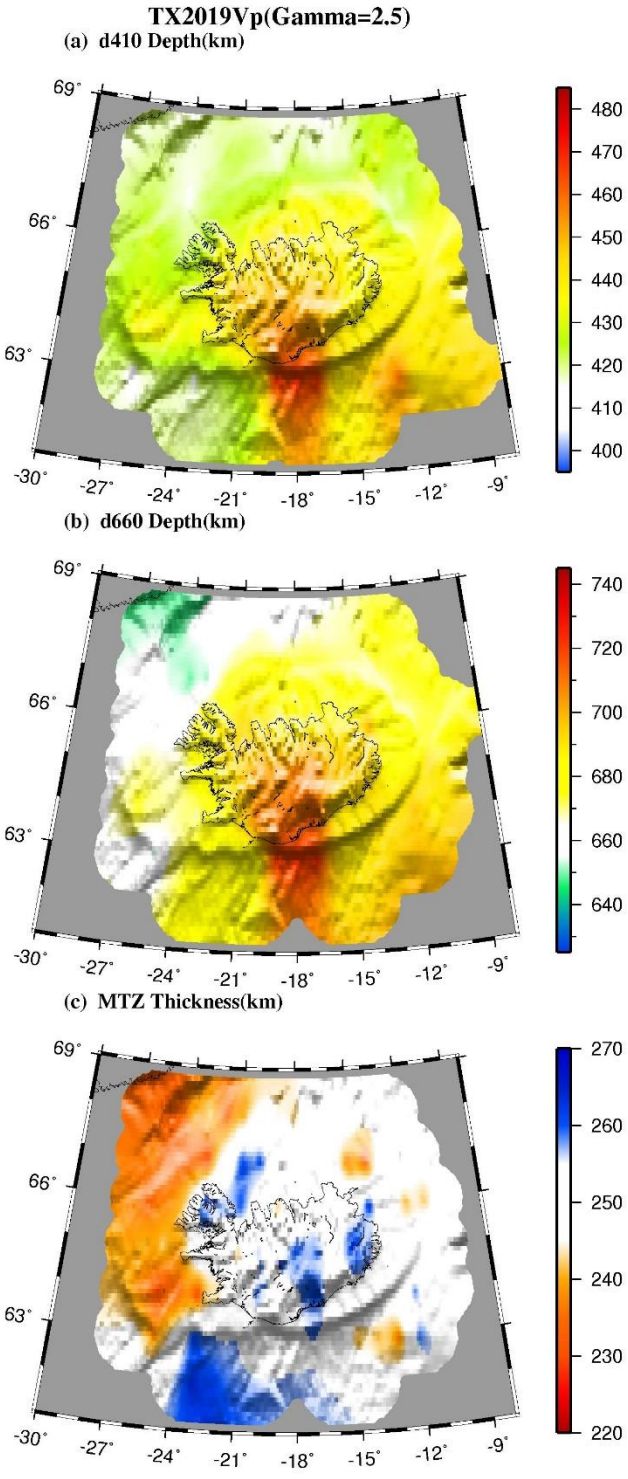

Figure S6. Correction results using the TX2019 Vp model with γ factors of 2.5.

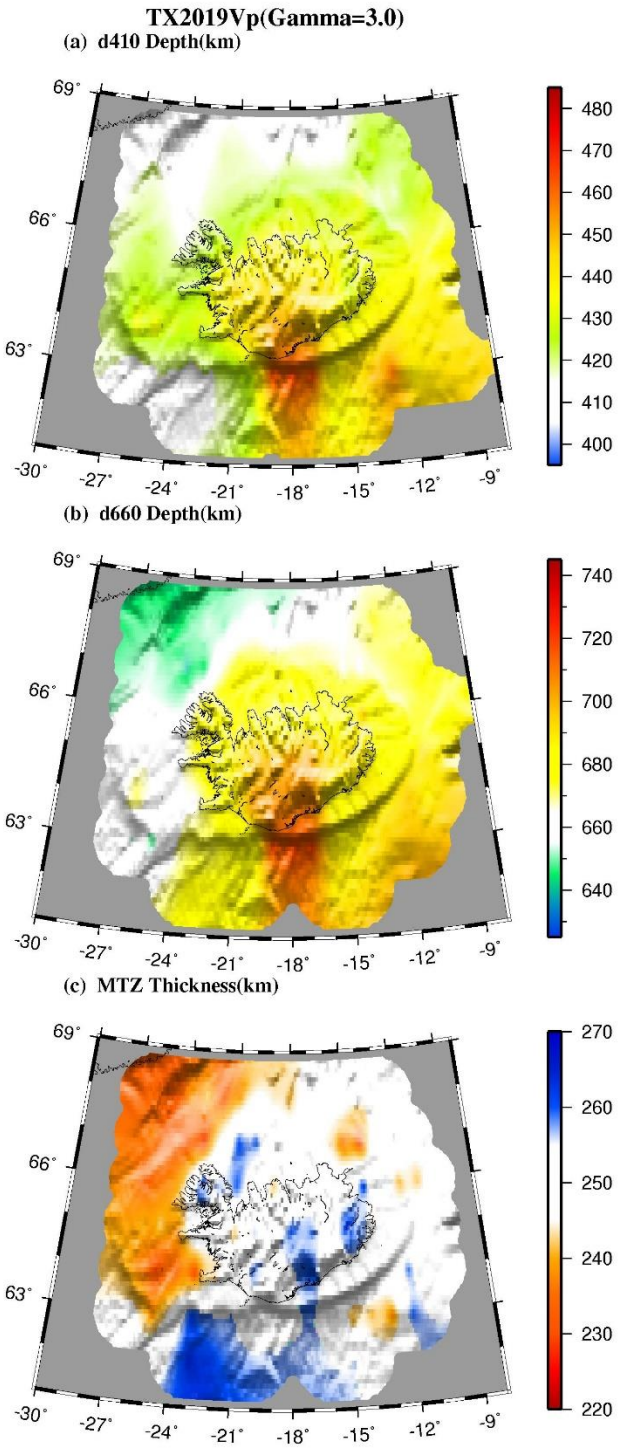

Figure S7. Correction results using the TX2019 Vp model with γ factors of 3.0.

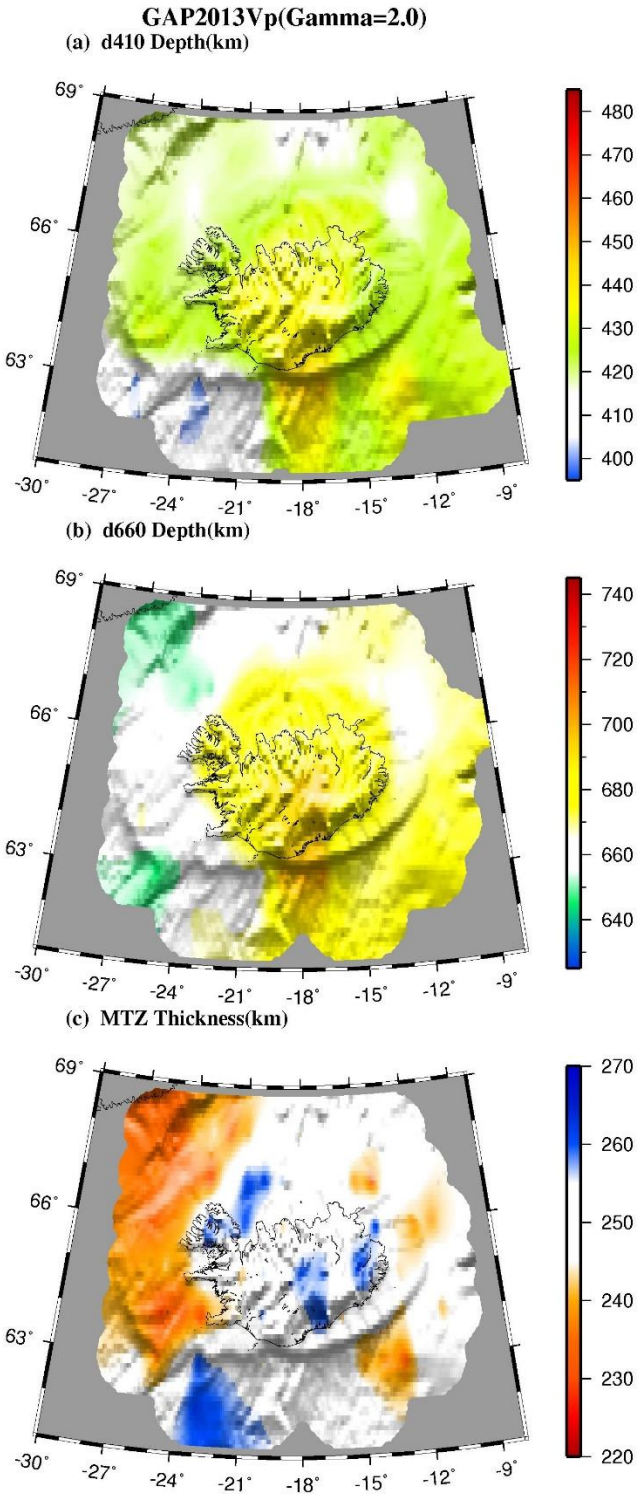

Figure S8. Correction results using the Vp models of GAP2013.

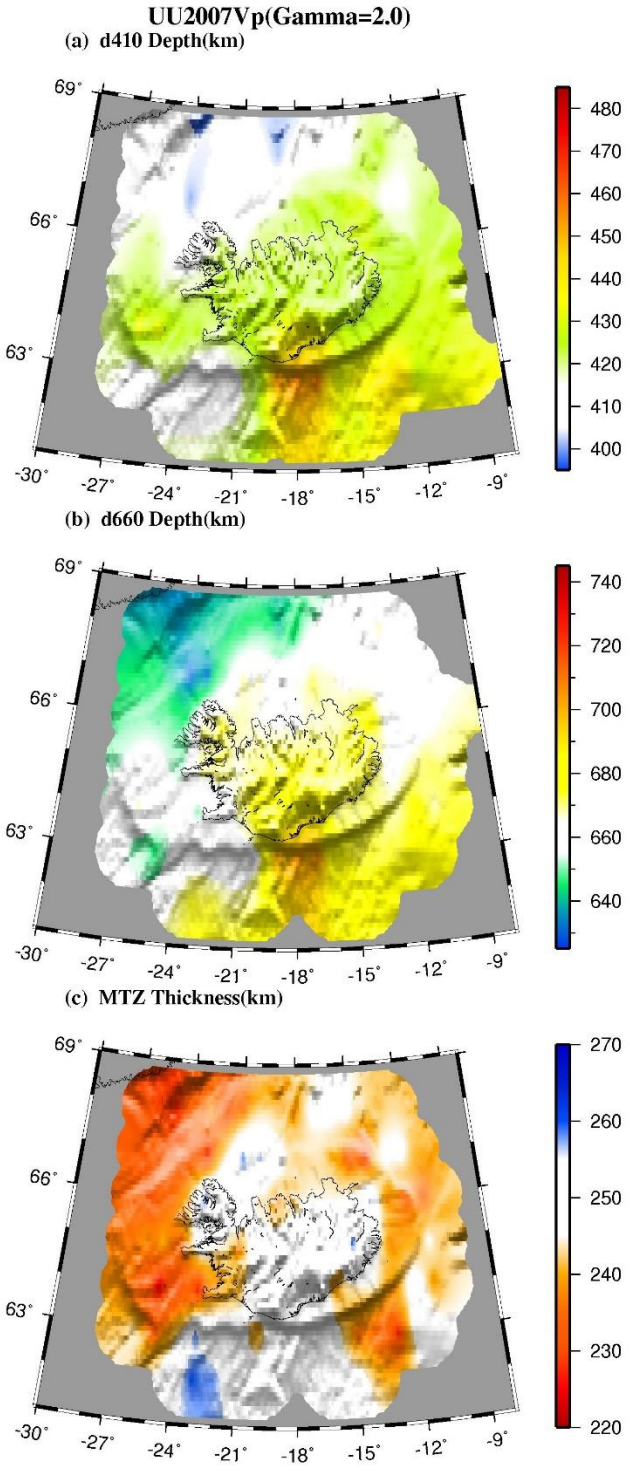

Figure S9. Correction results using the Vp models of UU2007.

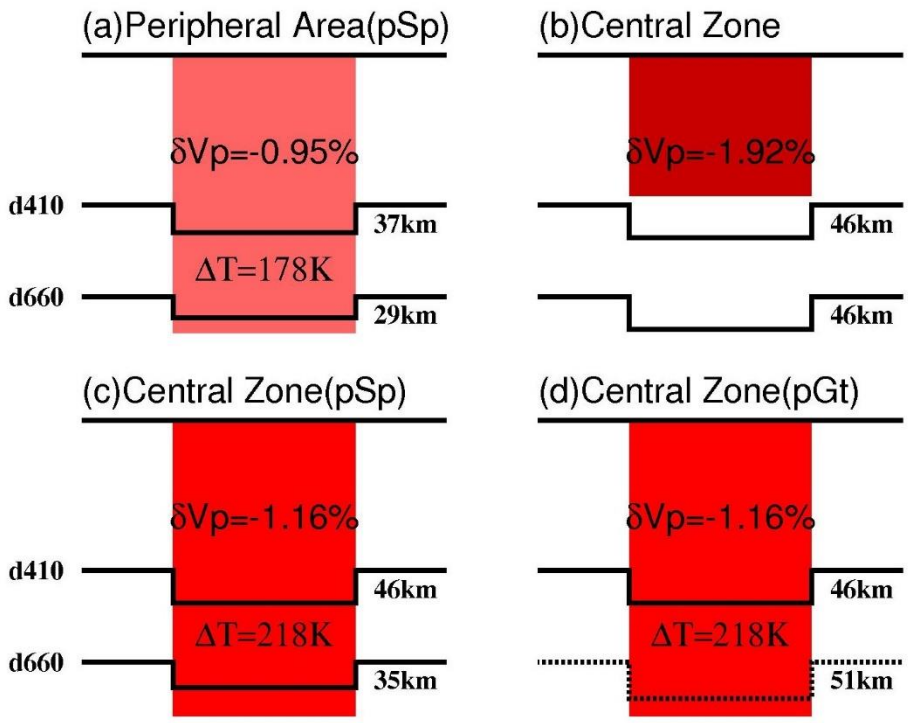

Figure S10. Schematic models to explain the observed apparent depressions of the MTZ discontinuities for the peripheral area (**a**) and the central zone (**b-d**). The wavespeed and temperature anomalies are estimated by the topography of the d410. The numbers at the d660 are the corrected amounts of the apparent depression for the d660 using the velocity and temperature anomalies. The dominant phase transition across the d660 for the models in **a-c** is post-spinel (pSp), and that for the model in **d** is post-garnet (pGt).

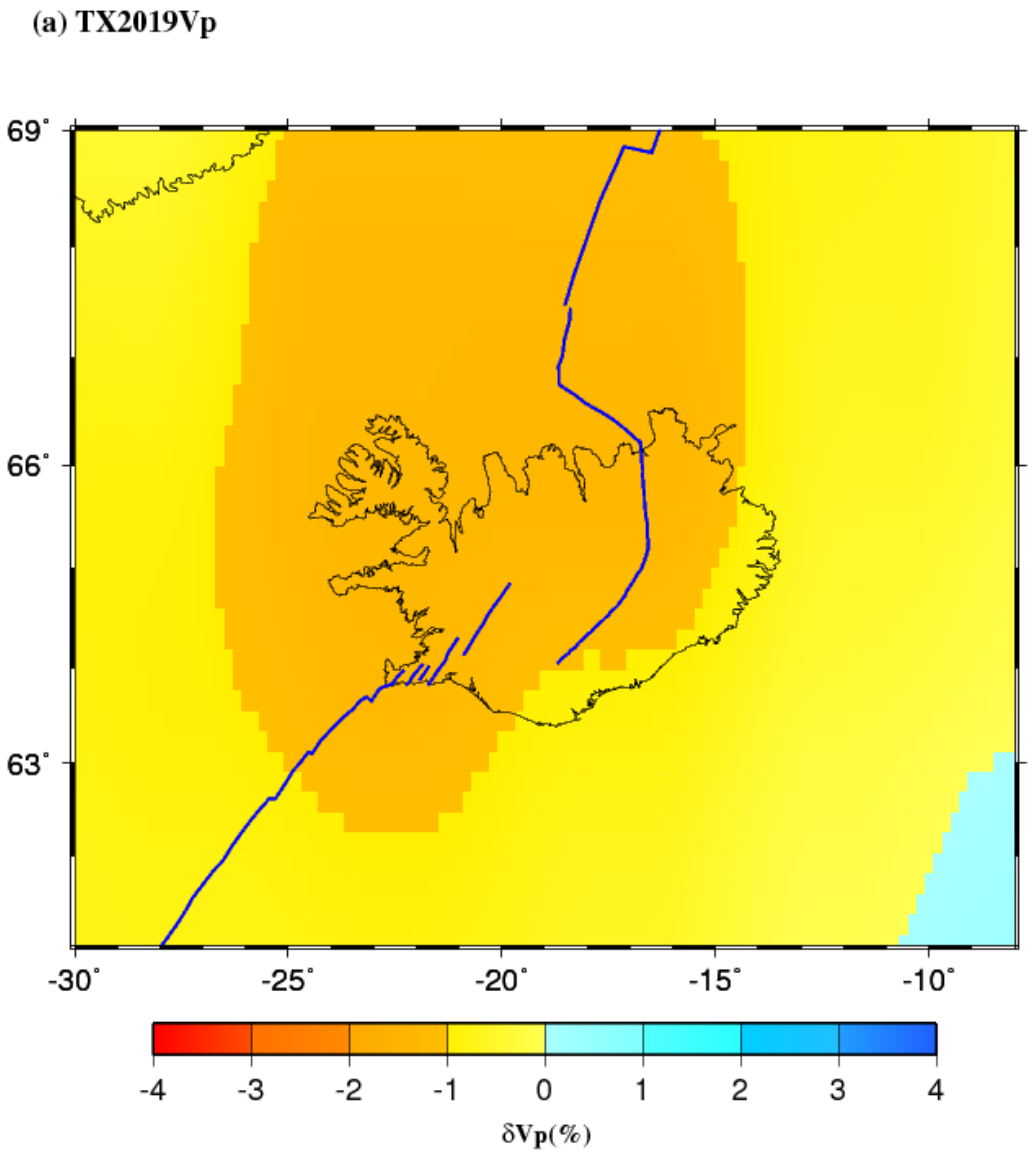

Figure S11. Mean wavespeed anomalies in the upper 410 km calculated using velocity model TX2019Vp.

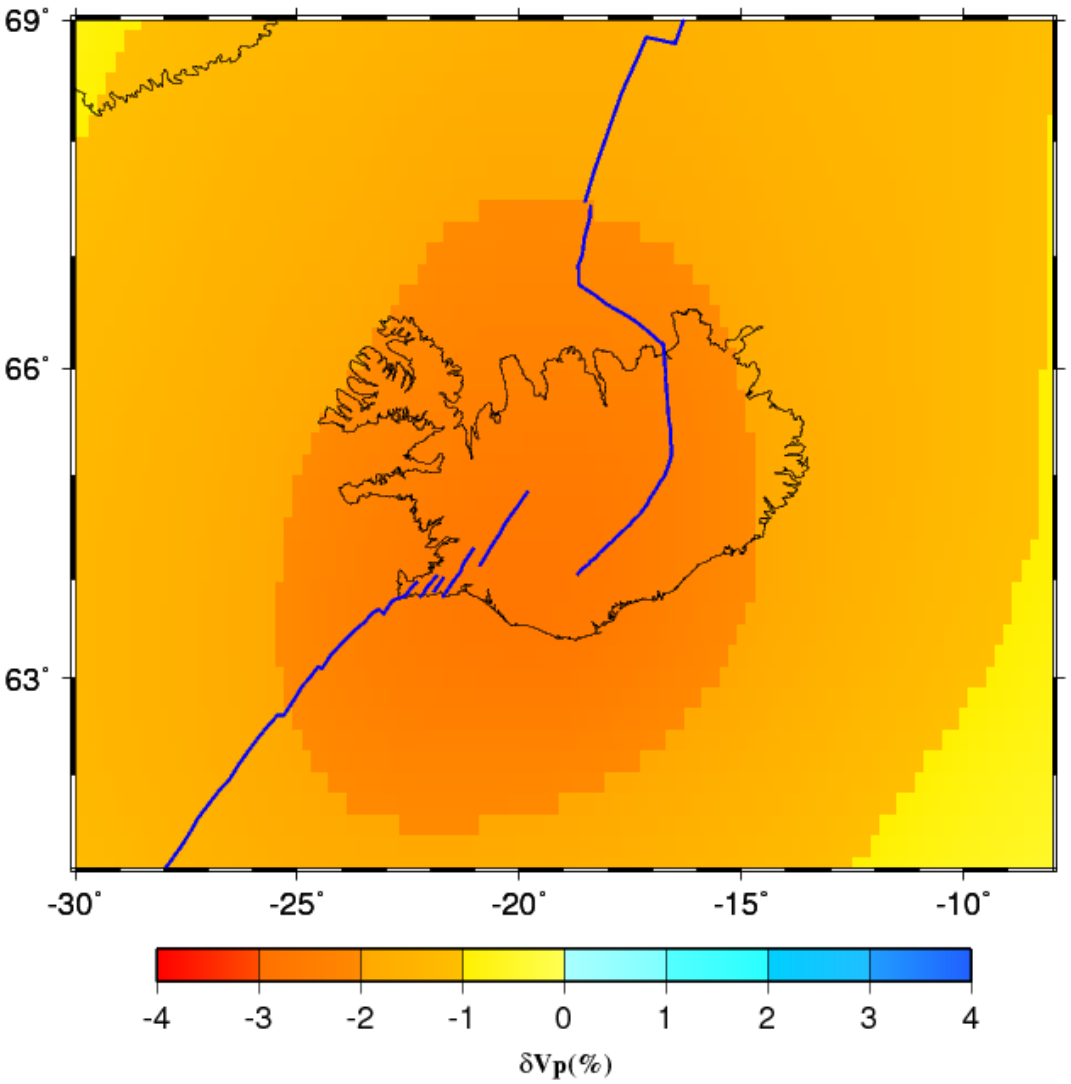

Figure S12. Mean wavespeed anomalies in the upper 410 km calculated using velocity model GAP2013Vp.

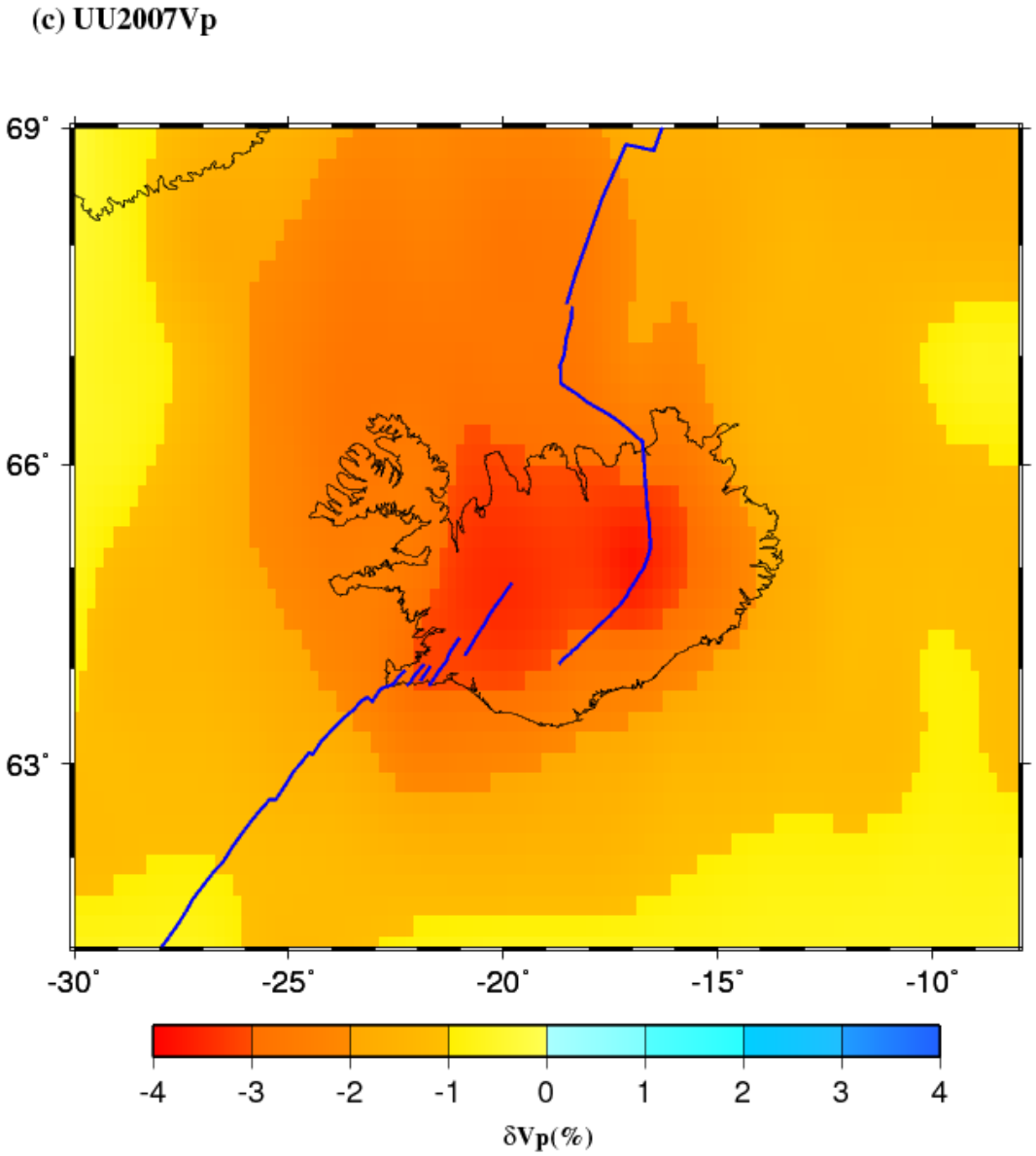

Figure S13. Mean wavespeed anomalies in the upper 410 km calculated using velocity model UU2007Vp .

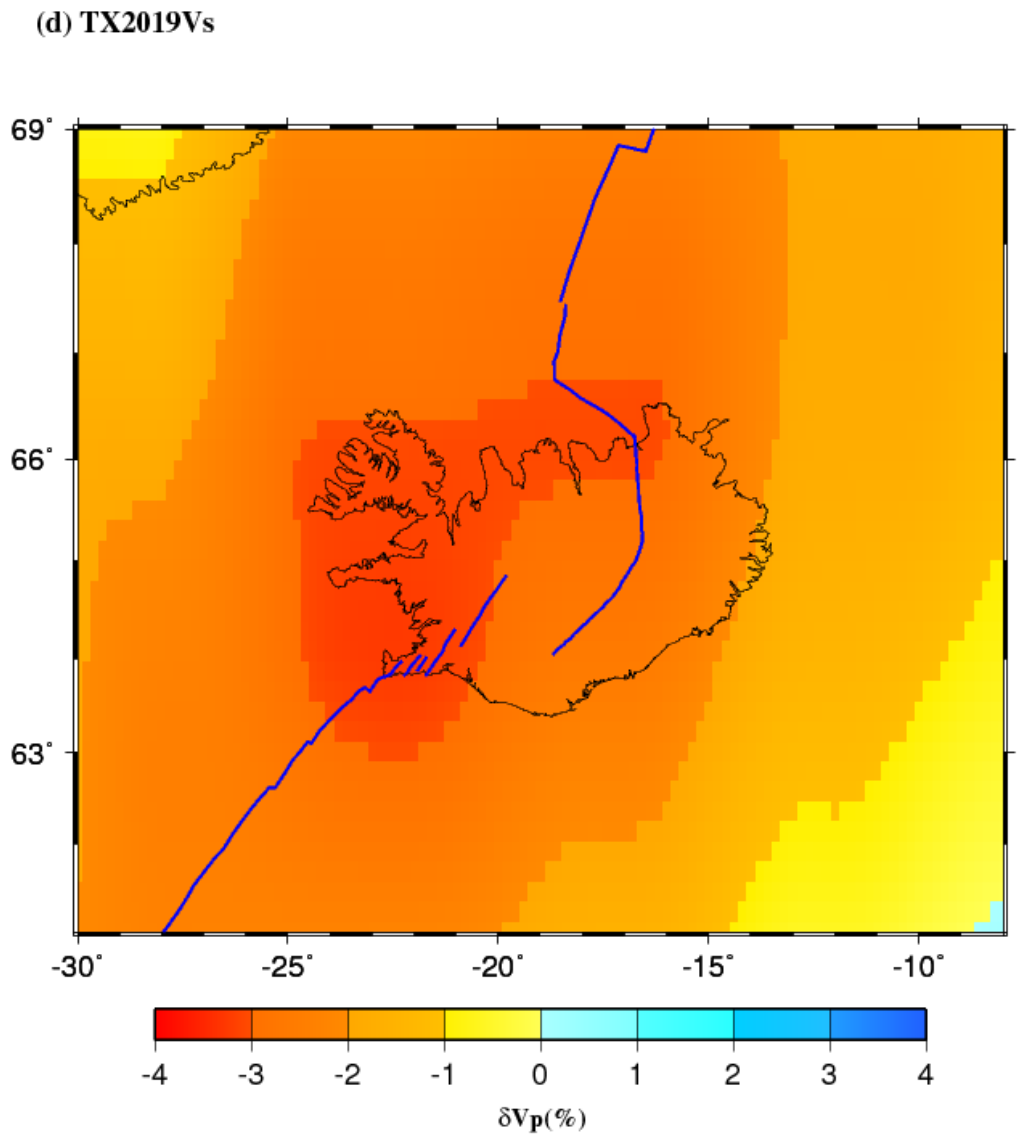

Figure S14. Mean wavespeed anomalies in the upper 410 km calculated using velocity model TX2019VpVs.

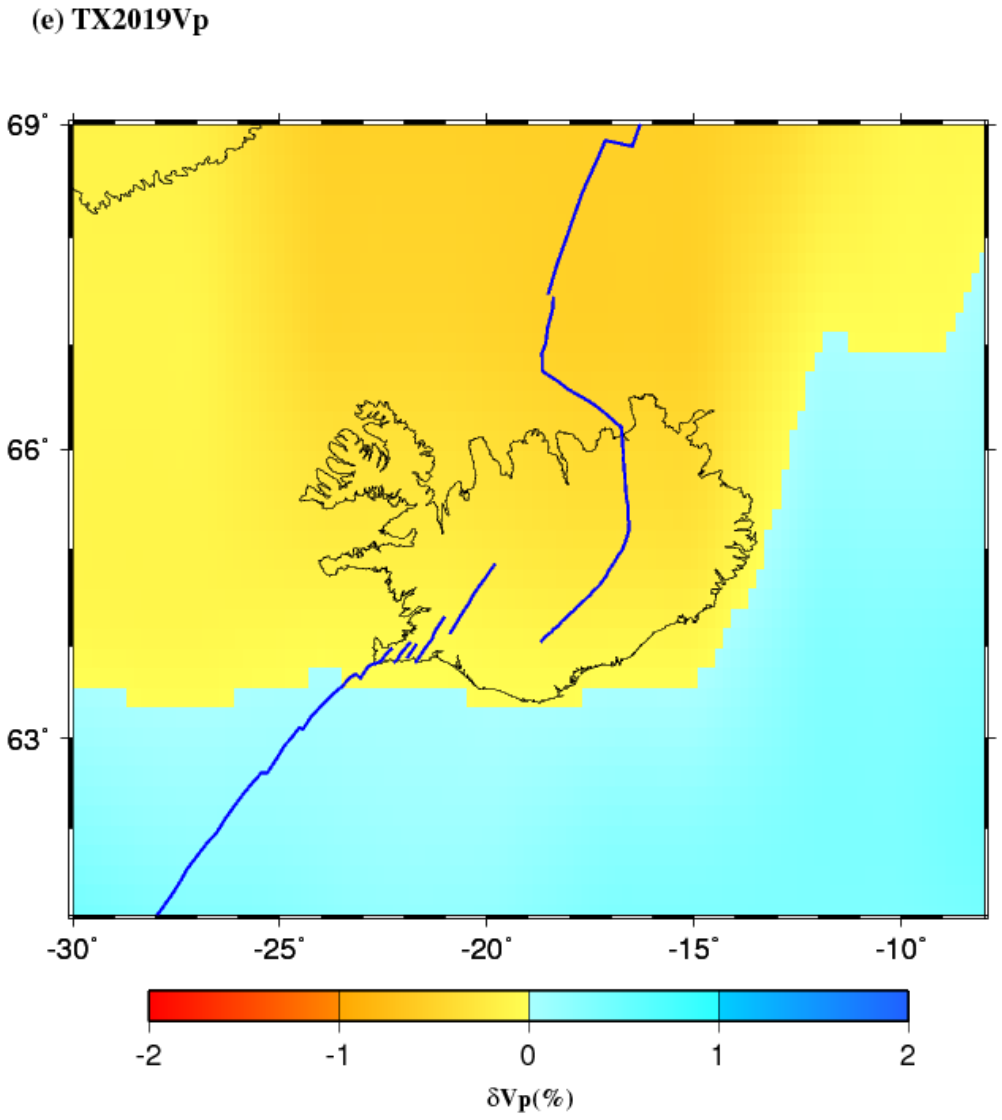

Figure S15. Mean wavespeed anomalies in the MTZ calculated using velocity model TX2019Vp.

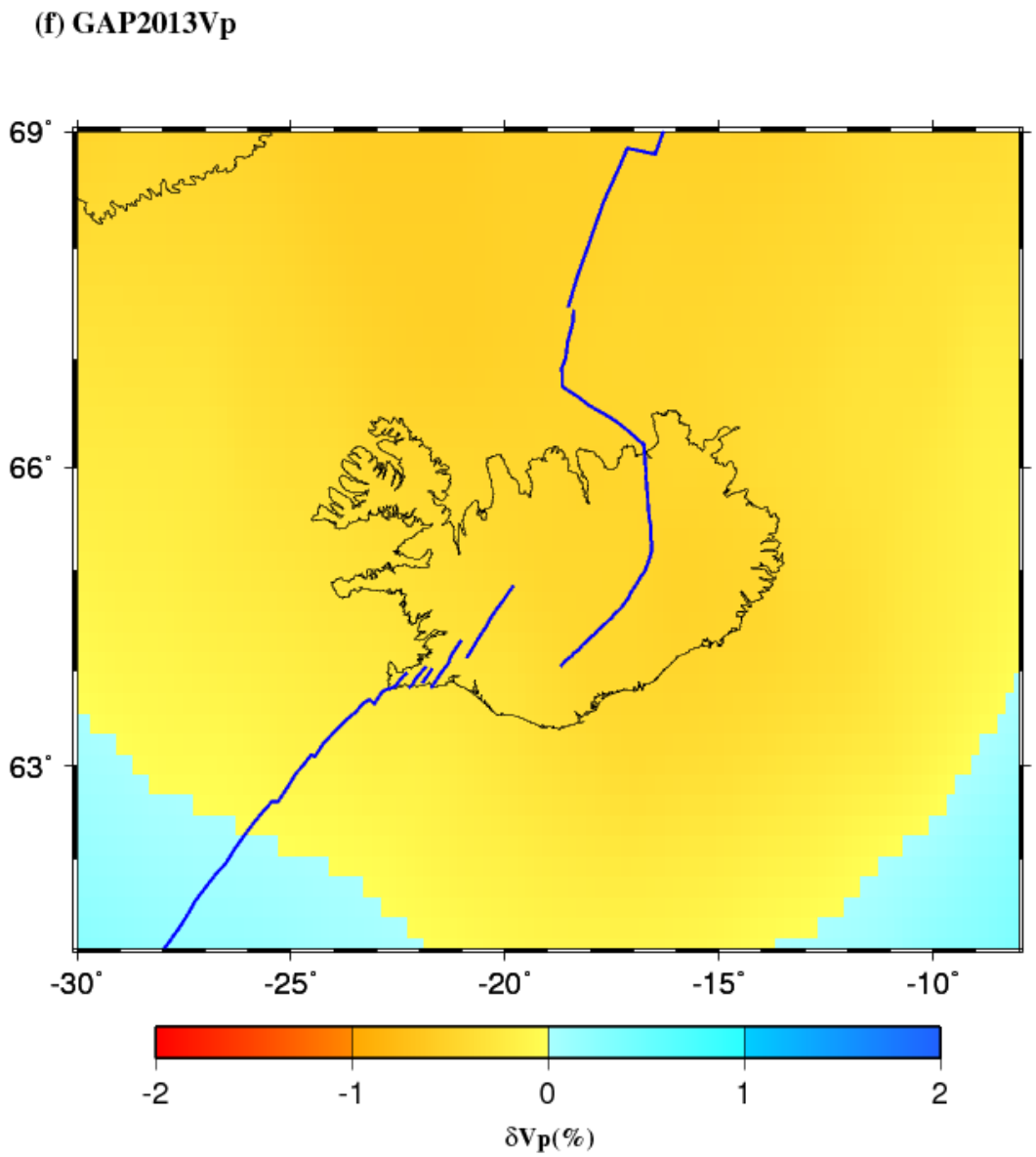

Figure S16. Mean wavespeed anomalies in the MTZ calculated using velocity model GAP2013Vp.

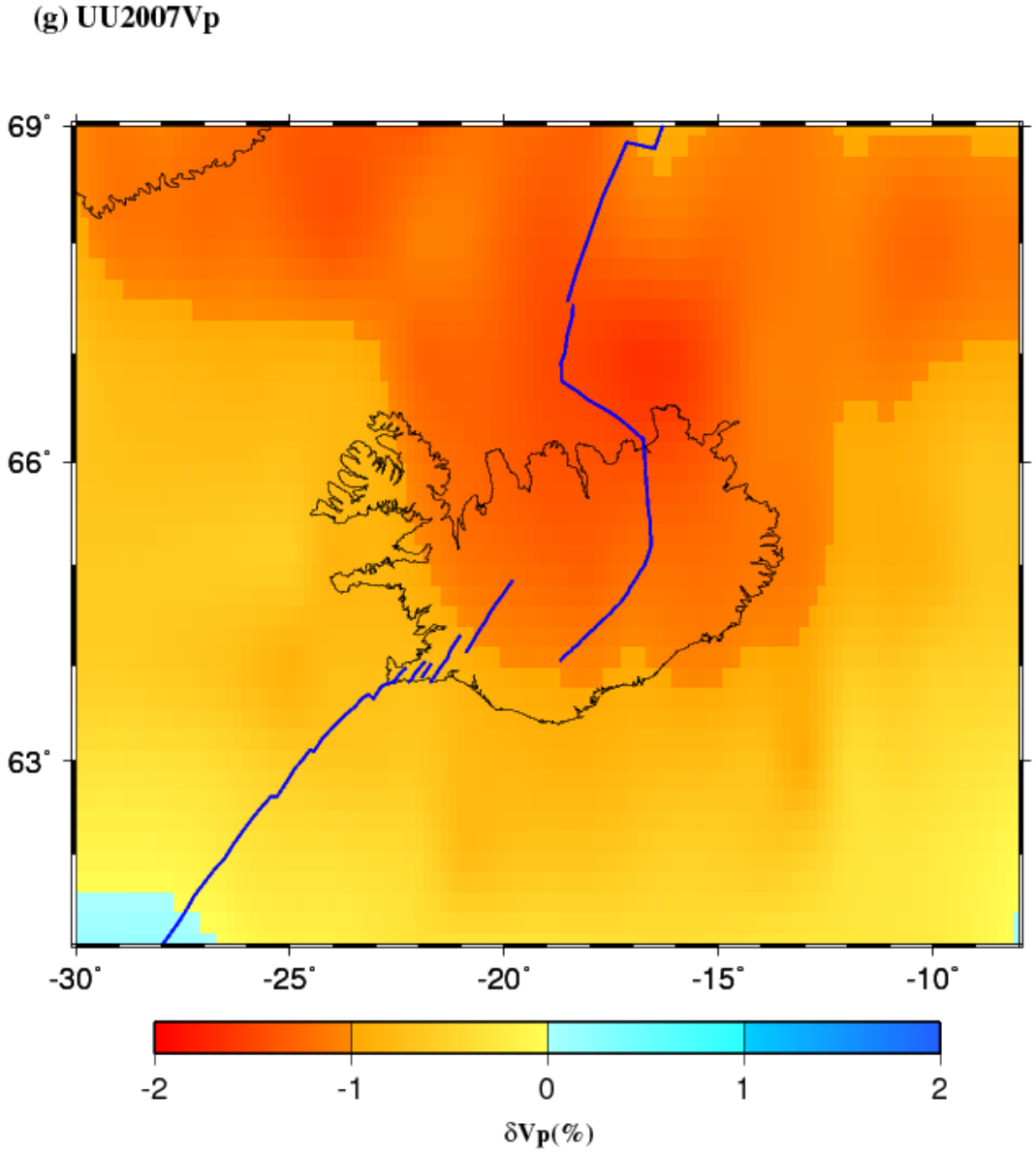

Figure S17. Mean wavespeed anomalies in the MTZ calculated using velocity model UU2007Vp.

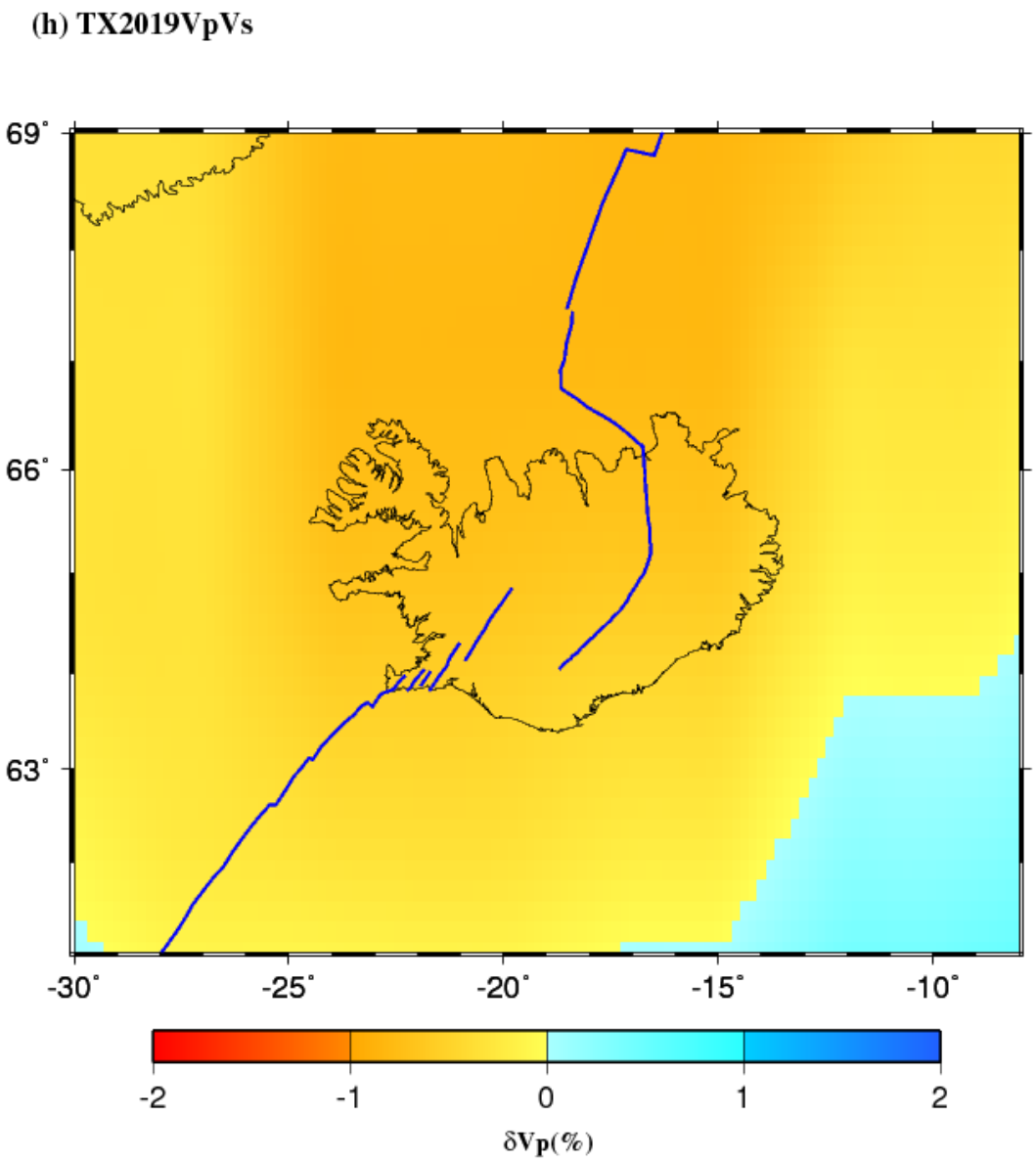

Figure S18. Mean wavespeed anomalies in the MTZ calculated using velocity model TX2019VpVs.

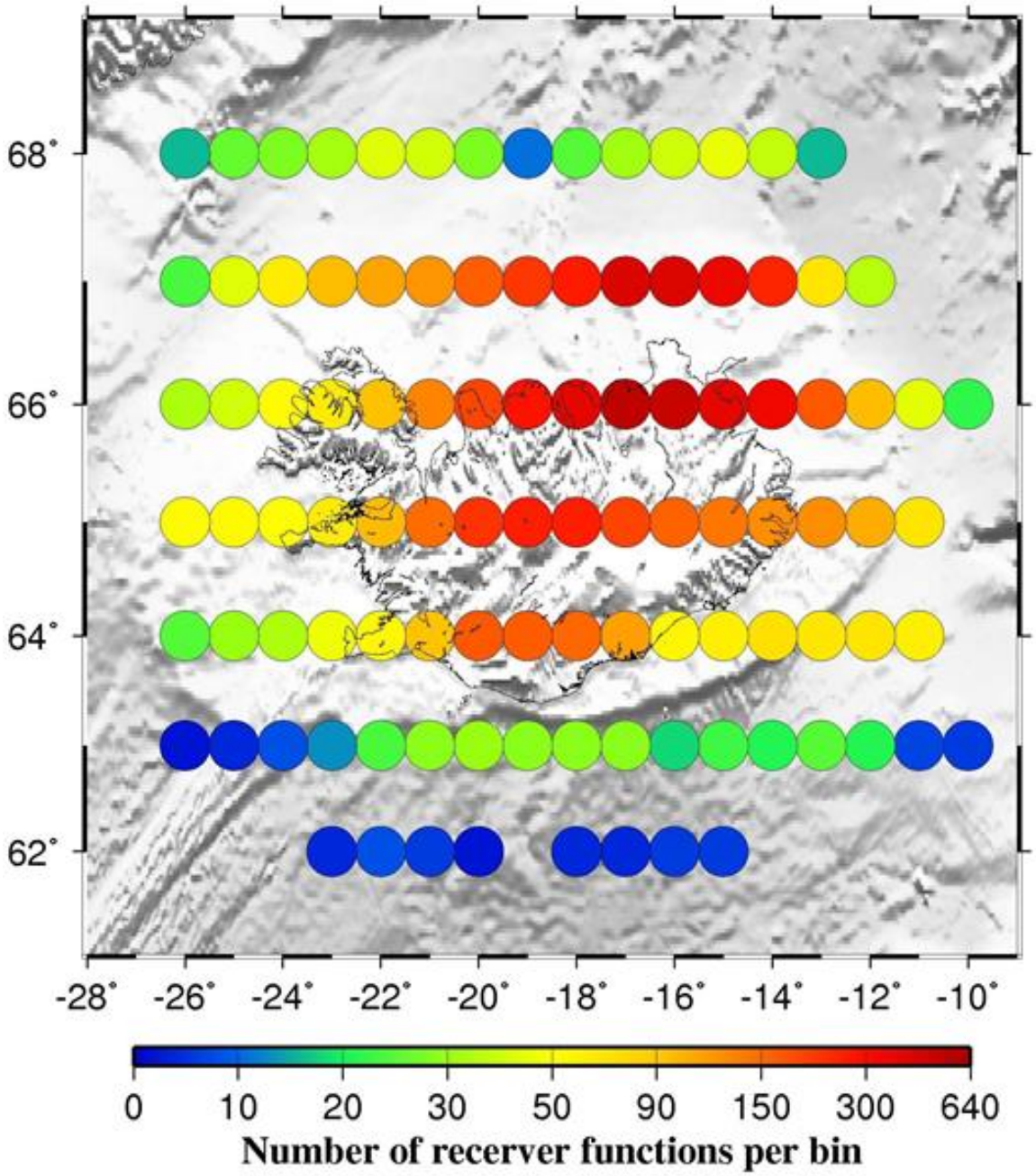

Figure S19. Distribution of the center of the circular bins (circles). For a given bin, the color of the circle shows the number of receiver functions in the bin.

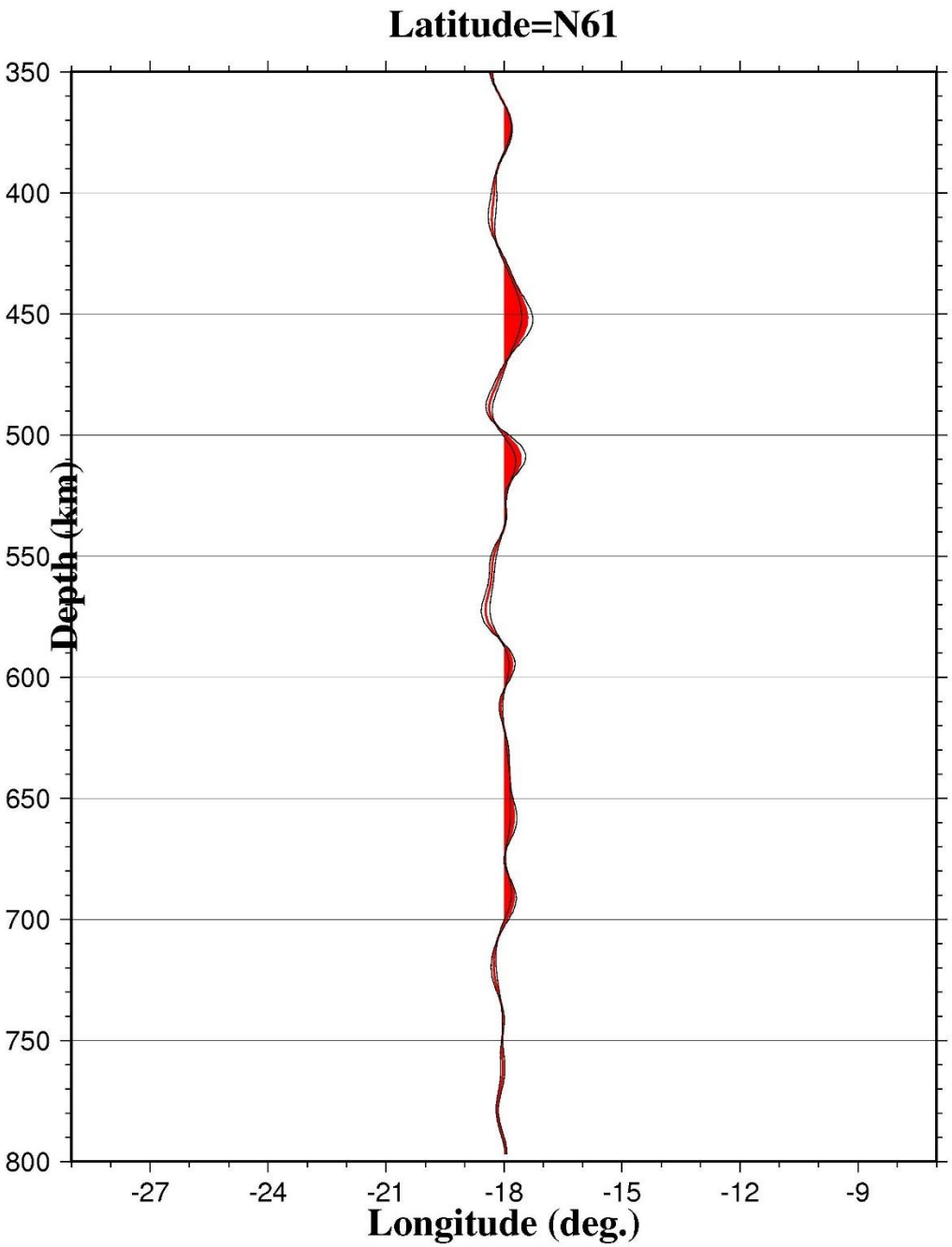

Figure S20. Trace plot along the latitude N61 profile.

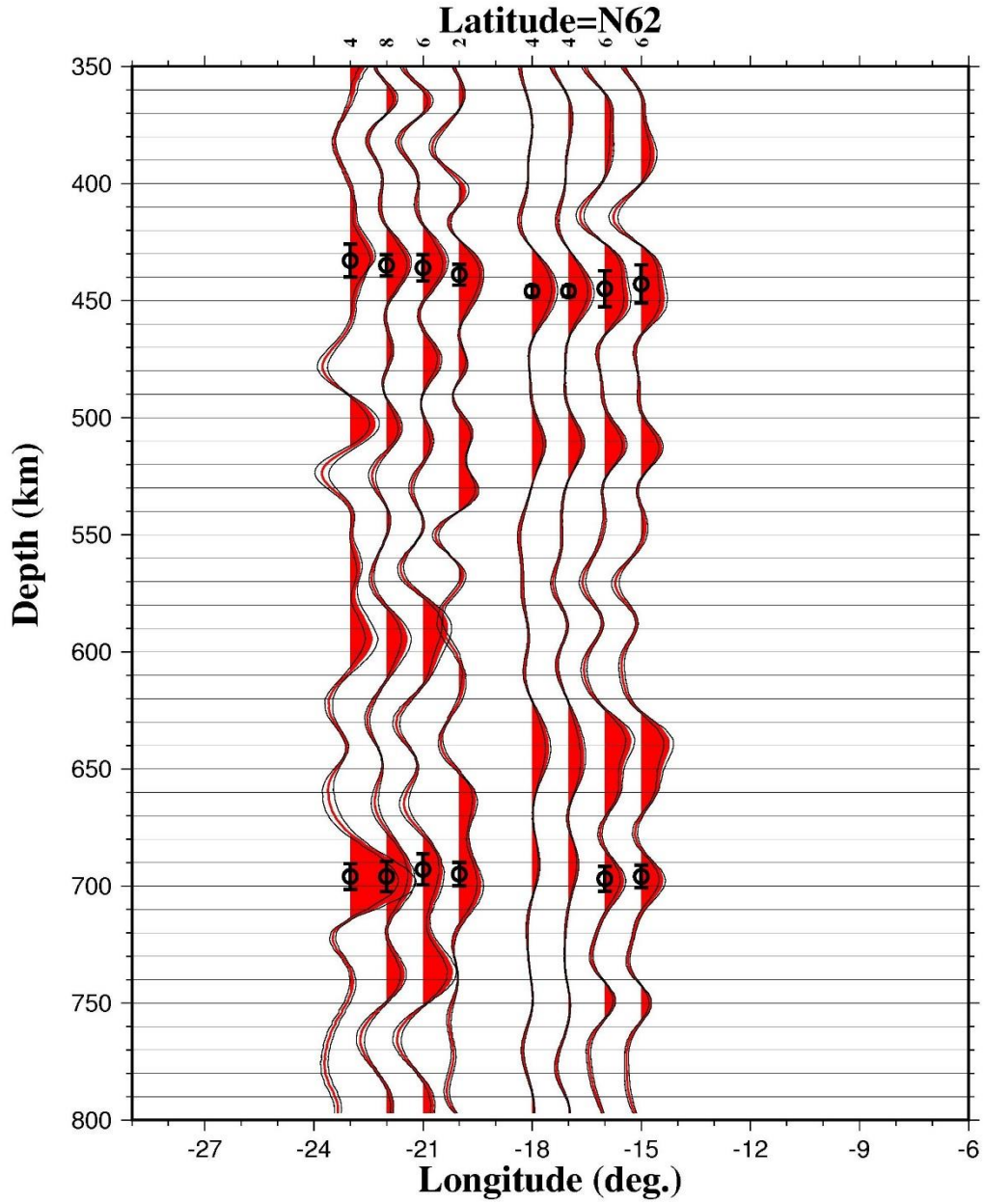

Figure S21. Trace plot along the latitude N62 profile. Black circles and bars indicate the picked peaks of the d410 and d660 arrivals and the standard deviations, respectively. Numbers above each trace show the numbers of receiver functions stacked in each bin.

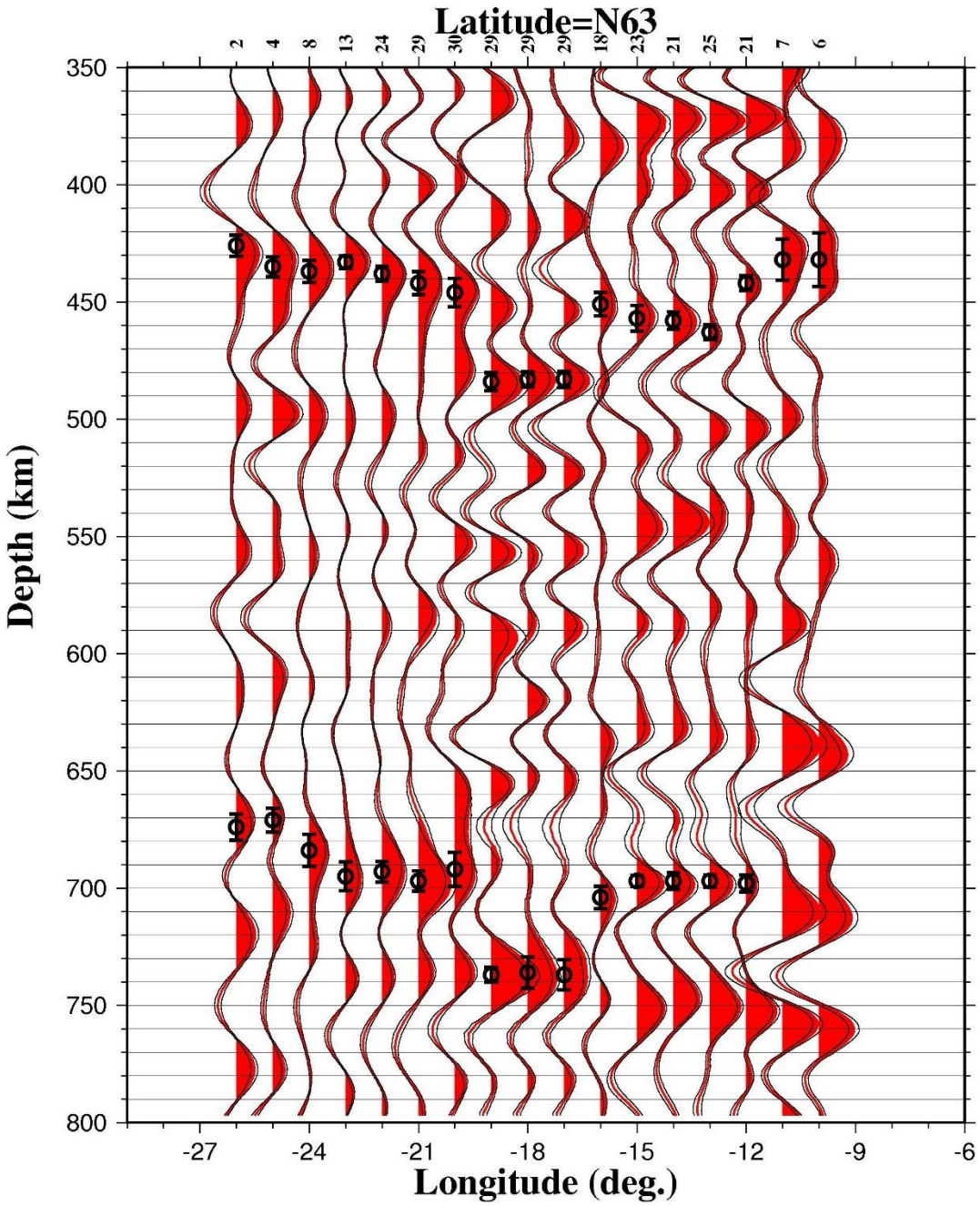

Figure S22. Trace plot along the latitude N63 profile. Black circles and bars indicate the picked peaks of the d410 and d660 arrivals and the standard deviations, respectively. Numbers above each trace show the numbers of receiver functions stacked in each bin.

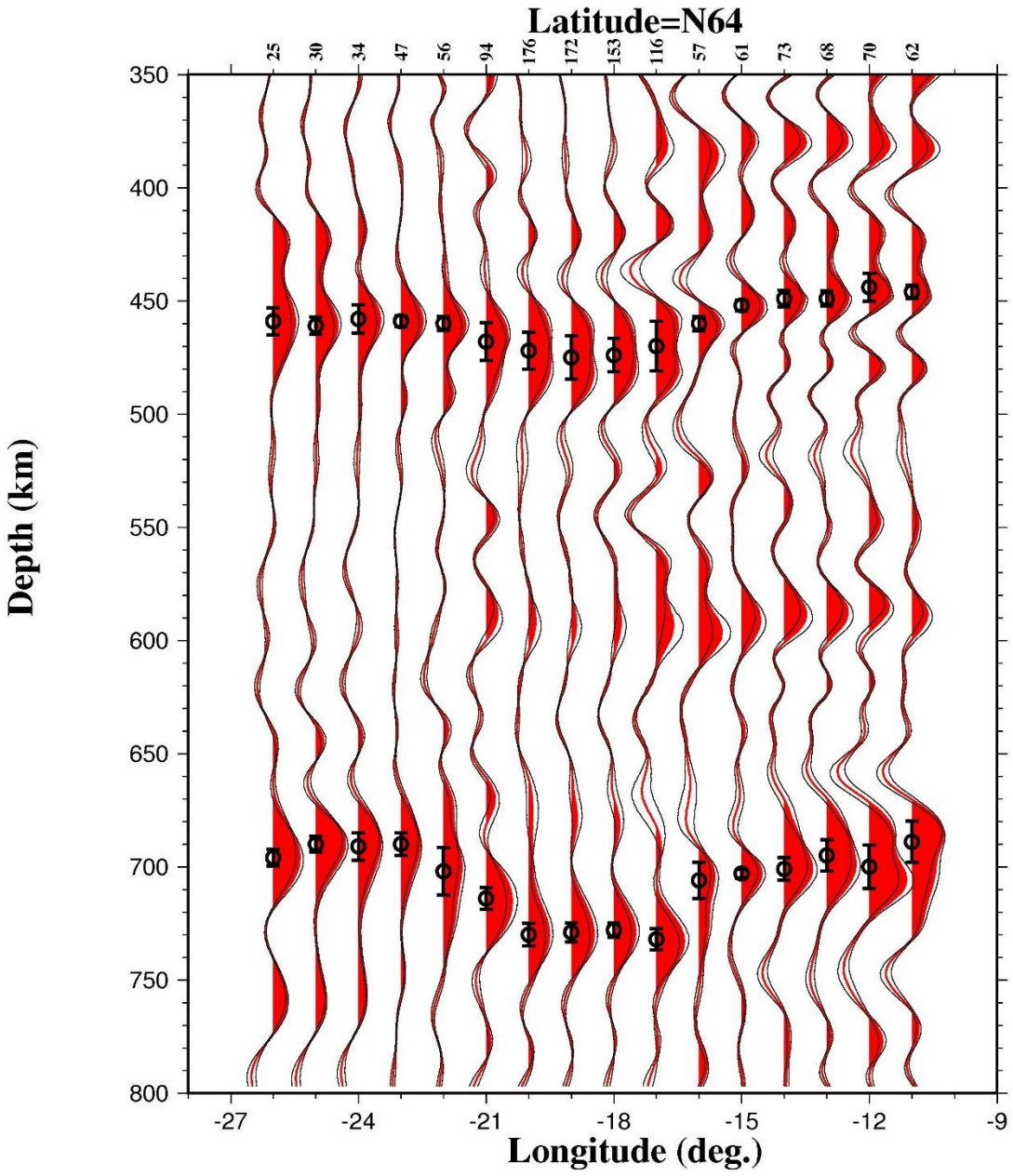

Figure S23. Trace plot along the latitude N64 profile. Black circles and bars indicate the picked peaks of the d410 and d660 arrivals and the standard deviations, respectively. Numbers above each trace show the numbers of receiver functions stacked in each bin.

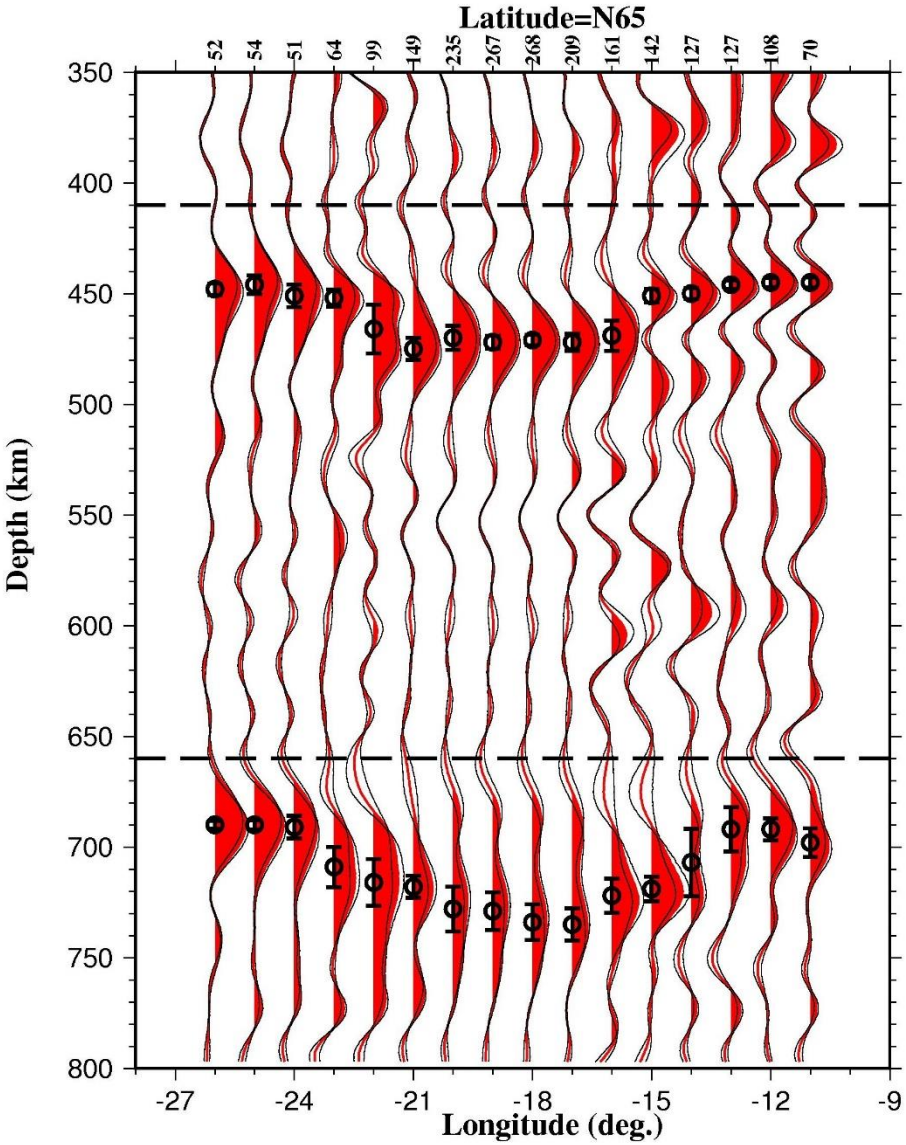

Figure S24. Trace plot along the latitude N65 profile. Black circles and bars indicate the picked peaks of the d410 and d660 arrivals and the standard deviations, respectively. Numbers above each trace show the numbers of receiver functions stacked in each bin.

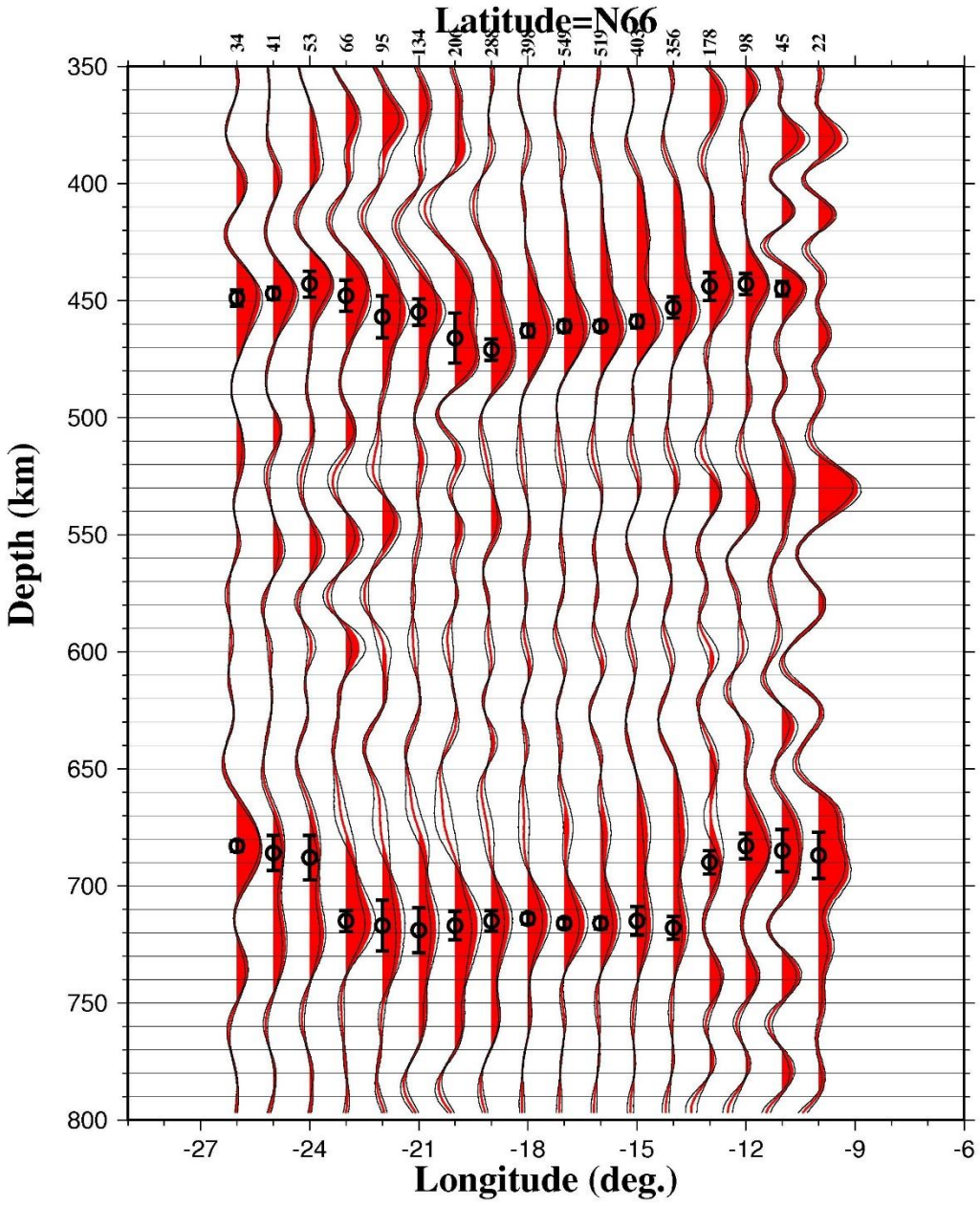

Figure S25. Trace plot along the latitude N66 profile. Black circles and bars indicate the picked peaks of the d410 and d660 arrivals and the standard deviations, respectively. Numbers above each trace show the numbers of receiver functions stacked in each bin.

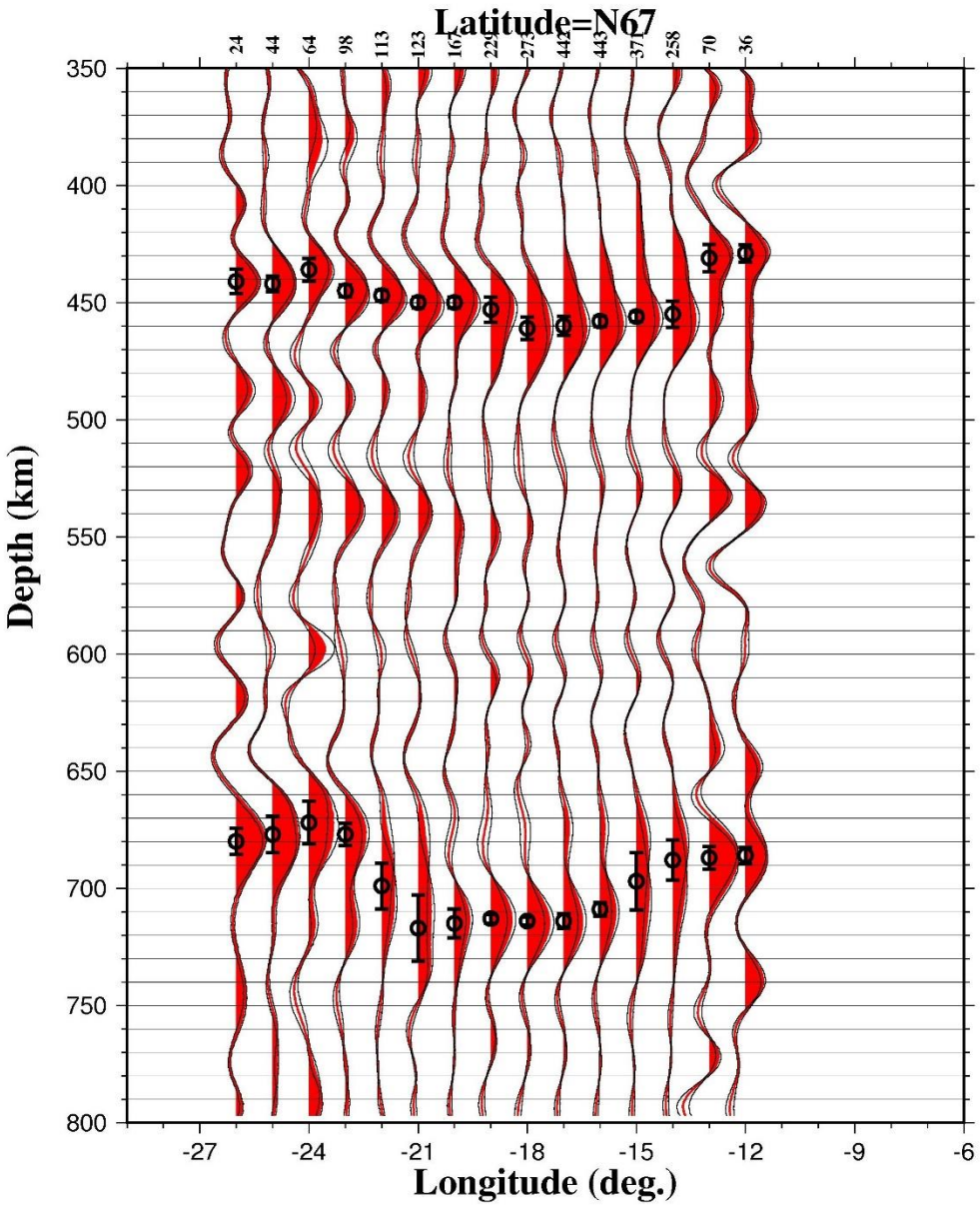

Figure S26. Trace plot along the latitude N67 profile. Black circles and bars indicate the picked peaks of the d410 and d660 arrivals and the standard deviations, respectively. Numbers above each trace show the numbers of receiver functions stacked in each bin.

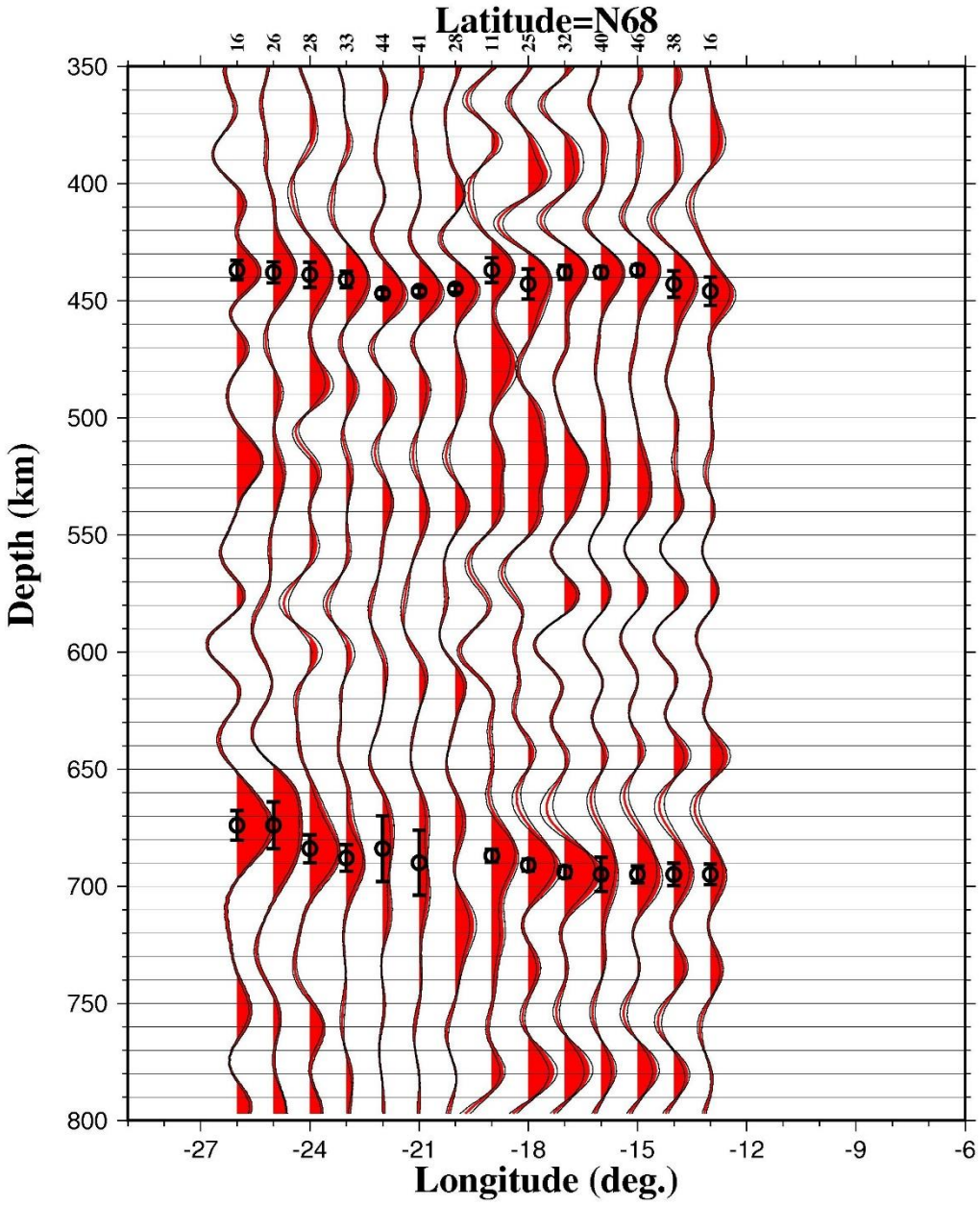

Figure S27. Trace plot along the latitude N68 profile. Black circles and bars indicate the picked peaks of the d410 and d660 arrivals and the standard deviations, respectively. Numbers above each trace show the numbers of receiver functions stacked in each bin.

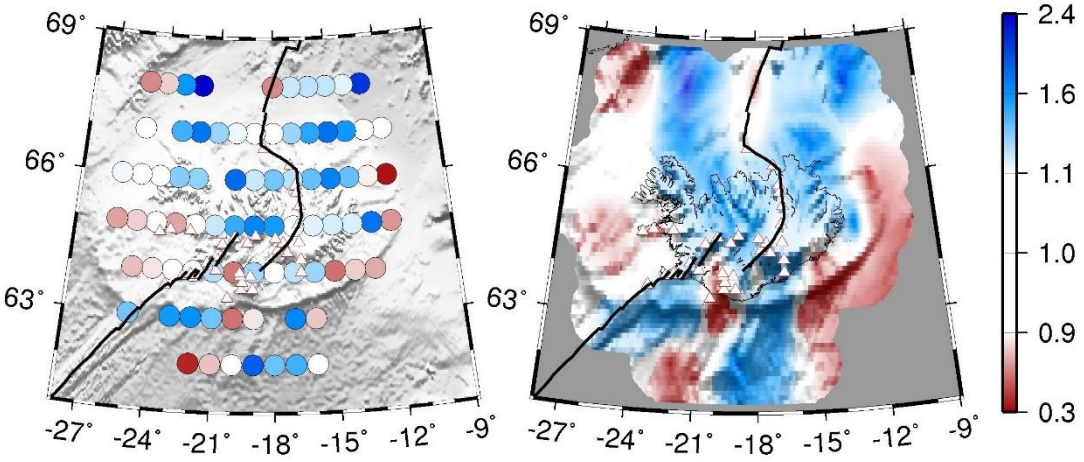

Figure S28. The spatial distribution of the amplitude ratio of the d410 over the d660 arrivals. The black lines indicate the mid-Atlantic Ridge (or the plate boundary), and the white triangles indicate the distribution of surface volcanoes. The blue area indicates the significant lower amplitude of the d660 arrivals with respect to that of the d410 arrivals caused by the attenuation effect of water on S waves. The white area and red area represent the areas with comparable and lower amplitude ratios, respectively. The possible causes of the smaller amplitude of the d660 with respect to that of the d410 are: (1) The water in the lower MTZ causes the effect of wave attenuation for the shear wave arrivals at the d660; (2) The longer pressure interval of the pGt transition comparing with that of the pSp transition; (3) The spacial variation of the d660 depths.

Table S1. Resulting apparent depths of the d410 and the d660 and the MTZ thickness for each bin. A value of zero means the measurement is non-existent.

Latitude	Longitude	d410 (km)	d660 (km)	MTZ Thickness(km)
63	-10	432	0	0
66	-10	0	687	0
63	-11	432	0	0
64	-11	446	689	242
65	-11	445	698	252

Table S1. Resulting apparent depths of the d410 and the d660 and the MTZ thickness for each bin (cont.).

66	-11	445	685	240
63	-12	442	698	256
64	-12	444	700	256
65	-12	445	692	247
66	-12	443	683	240
67	-12	429	686	256
63	-13	463	697	234
64	-13	449	695	246
65	-13	446	692	245
66	-13	444	690	246
67	-13	431	687	256
68	-13	446	695	249
63	-14	458	697	239
64	-14	449	701	251
65	-14	450	707	257
66	-14	453	718	265
67	-14	455	688	232
68	-14	443	695	251
62	-15	443	696	253
63	-15	457	697	240
64	-15	452	703	250

Table S1. Resulting apparent depths of the d410 and the d660 and the MTZ thickness for each bin (cont.).

65	-15	451	719	267
66	-15	459	715	256
67	-15	456	697	240
68	-15	437	695	258
62	-16	445	697	252
63	-16	451	704	252
64	-16	460	706	246
65	-16	469	722	253
66	-16	461	716	254
67	-16	458	709	251
68	-16	438	695	257
62	-17	446	0	0
63	-17	483	737	254
64	-17	470	732	262
65	-17	472	735	262
66	-17	461	716	254
67	-17	460	714	253
68	-17	438	694	256
68	-18	443	691	247
67	-18	461	714	253
66	-18	463	714	251

Table S1. Resulting apparent depths of the d410 and the d660 and the MTZ thickness for each bin (cont.).

65	-18	471	734	263
64	-18	474	728	254
63	-18	483	736	253
62	-18	446	0	0
68	-19	437	687	249
67	-19	453	713	260
66	-19	471	715	244
65	-19	472	729	257
64	-19	475	729	254
63	-19	484	737	253
68	-20	445	0	0
67	-20	450	715	265
66	-20	466	717	251
65	-20	470	728	258
64	-20	472	730	258
63	-20	446	692	246
62	-20	439	695	256
68	-21	446	690	243
67	-21	450	717	267
66	-21	455	719	264
65	-21	475	718	243

Table S1. Resulting apparent depths of the d410 and the d660 and the MTZ thickness for each bin (cont.).

64	-21	468	714	246
63	-21	442	697	255
62	-21	436	693	256
68	-22	447	684	237
67	-22	447	699	251
66	-22	457	717	260
65	-22	466	716	250
64	-22	460	702	241
63	-22	438	693	254
68	-23	441	688	247
62	-22	435	696	260
67	-23	445	677	232
66	-23	448	715	266
65	-23	452	709	257
64	-23	459	690	231
68	-24	439	684	245
63	-23	433	695	262
67	-24	436	672	236
62	-23	433	696	262
66	-24	443	688	245
65	-24	451	691	240

Table S1. Resulting apparent depths of the d410 and the d660 and the MTZ thickness for each bin (cont.).

68	-25	438	674	236
64	-24	458	691	232
67	-25	442	677	235
63	-24	437	684	247
66	-25	447	686	239
65	-25	446	690	243
68	-26	437	674	236
64	-25	461	690	228
67	-26	441	680	238
63	-25	435	671	235
66	-26	449	683	233
65	-26	448	690	242
64	-26	459	696	236
63	-26	426	674	248

REFERENCES

1. White, R. & McKenzie, D. Magmatism at rift zones: The generation of volcanic continental margins and flood basalts. *J. Geophys. Res.* **94**, 7685 (1989).

2. Steinberger, B., Bredow, E., Lebedev, S., Schaeffer, A. & Torsvik, T. H. Widespread volcanism in the Greenland–North Atlantic region explained by the Iceland plume. *Nat. Geosci.* **12**, 61–68 (2019).

3. Ruedas, T., Marquart, G. & Schmeling, H. Iceland: The current picture of a ridge-centred mantle plume. in *Mantle Plumes: A Multidisciplinary Approach* 71–126 (Springer Berlin Heidelberg, 2007). doi:10.1007/978-3-540-68046-8_3.

4. Foulger, G. R. *et al.* Seismic tomography shows that upwelling beneath Iceland is confined to the upper mantle. *Geophys. J. Int.* **146**, 504–530 (2001).

5. Foulger, G. R. *et al.* The seismic anomaly beneath Iceland extends down to the mantle transition zone and no deeper. *Geophys. J. Int.* **142**, F1–F5 (2000).

6. Wolfe, C. J., Th. Bjarnason, I., VanDecar, J. C. & Solomon, S. C. Seismic structure of the Iceland mantle plume. *Nature* **385**, 245–247 (1997).

7. Allen, R. M. *et al.* Imaging the mantle beneath Iceland using integrated seismological techniques. *J. Geophys. Res. Solid Earth* **107**, ESE 3-1-ESE 3-16 (2002).

8. Keller, W. R., Anderson, D. L. & Clayton, R. W. Resolution of tomographic models of the mantle beneath Iceland. *Geophys. Res. Lett.* **27**, 3993–3996 (2000).

9. Foulger, G. R. *et al.* Caveats on tomographic images. *Terra Nov.* **25**, 259–281 (2013).

10. Bijwaard, H. & Spakman, W. Tomographic evidence for a narrow whole mantle plume below Iceland. *Earth Planet. Sci. Lett.* **166**, 121–126 (1999).

11. Ritsema, J. Complex Shear Wave Velocity Structure Imaged Beneath Africa and Iceland. *Science (80-.).* **286**, 1925–1928 (1999).

12. Rickers, F., Fichtner, A. & Trampert, J. The Iceland–Jan Mayen plume system and its impact on mantle dynamics in the North Atlantic region: Evidence from full-waveform inversion. *Earth Planet. Sci. Lett.* **367**, 39–51 (2013).

13. French, S. W. & Romanowicz, B. Broad plumes rooted at the base of the Earth's mantle beneath major hotspots. *Nature* **525**, 95–99 (2015).

14. Liu, H. *et al.* The combined effects of post-spinel and post-garnet phase transitions on mantle plume dynamics. *Earth Planet. Sci. Lett.* **496**, 80–88 (2018).

15. Bina, C. R. & Helffrich, G. Phase transition Clapeyron slopes and transition zone seismic discontinuity topography. *J. Geophys. Res.* **99**, 15853 (1994).

16. Fei, Y. *et al.* Experimentally determined postspinel transformation boundary in Mg 2 SiO 4 using MgO as an internal pressure standard and its geophysical implications. *J. Geophys. Res. Solid Earth* **109**, (2004).

17. Hirose, K. Phase transitions in pyrolitic mantle around 670-km depth: Implications for upwelling of plumes from the lower mantle. *J. Geophys. Res. Solid Earth* **107**, ECV 3-1-ECV 3-13 (2002).

18. Shen, Y., Solomon, S. C., Bjarnason, I. T. & Purdy, G. M. Hot mantle transition zone beneath Iceland and the adjacent Mid-Atlantic Ridge inferred from P-to-S conversions at the 410- and 660-km discontinuities. *Geophys. Res. Lett.* **23**, 3527–3530 (1996).

19. Shen, Y. *et al.* Seismic evidence for a tilted mantle plume and north–south mantle flow beneath Iceland. *Earth Planet. Sci. Lett.* **197**, 261–272 (2002).

20. Du, Z., Vinnik, L. P. & Foulger, G. R. Evidence from P-to-S mantle converted waves for a flat '660-km' discontinuity beneath Iceland. *Earth Planet. Sci. Lett.* **241**, 271–280 (2006).

21. Jenkins, J., Cottaar, S., White, R. S. & Deuss, A. Depressed mantle discontinuities beneath Iceland: Evidence of a garnet controlled 660 km discontinuity? *Earth Planet. Sci. Lett.* **433**, 159–168 (2016).

22. Lu, C., Grand, S. P., Lai, H. & Garnero, E. J. TX2019slab: A New P and S Tomography Model Incorporating Subducting Slabs. *J. Geophys. Res. Solid Earth* **124**, 11549–11567 (2019).

23. Obayashi, M. *et al.* Finite frequency whole mantle P wave tomography: Improvement of subducted slab images. *Geophys. Res. Lett.* **40**, 5652–5657 (2013).

24. Amaru, M. L. Global travel time tomography with 3-D reference models. *Geol. Ultraiectina* **274**, 174p (2007).

25. Lawrence, J. F. & Shearer, P. M. A global study of transition zone thickness using receiver functions. *J. Geophys. Res. Solid Earth* **111**, n/a-n/a (2006).

26. Andrews, J. & Deuss, A. Detailed nature of the 660 km region of the mantle from global receiver function data. *J. Geophys. Res. Solid Earth* **113**, (2008).

27. Deal, M. M., Nolet, G. & van der Hilst, R. D. Slab temperature and thickness from seismic tomography: 1. Method and application to Tonga. *J. Geophys. Res. Solid Earth* **104**, 28789–28802 (1999).

28. Ito, E. & Katsura, T. A temperature profile of the mantle transition zone. *Geophys. Res. Lett.* **16**, 425–428 (1989).

29. Ishii, T., Kojitani, H. & Akaogi, M. Phase relations and mineral chemistry in pyrolitic mantle at 1600–2200 °C under pressures up to the uppermost lower mantle: Phase transitions around the 660-km discontinuity and dynamics of upwelling hot plumes. *Phys. Earth Planet. Inter.* **274**, 127–137 (2018).

30. Ye, Y., Gu, C., Shim, S.-H., Meng, Y. & Prakapenka, V. The postspinel boundary in pyrolitic compositions determined in the laser-heated diamond anvil cell. *Geophys. Res. Lett.* **41**, 3833–3841 (2014).

31. Gao, S. S. & Liu, K. H. Mantle transition zone discontinuities beneath the contiguous United States. *J. Geophys. Res. Solid Earth* **119**, 6452–6468 (2014).

32. Charles J. Ammon. The isolation of receiver effects from teleseismic P waveforms. *Bull. Seismol. Soc. Am.* **81 (6)**, 2504–2510 (1991).

33. Gao, S. S. & Liu, K. H. Imaging mantle discontinuities using multiply-reflected P-to-S conversions. *Earth Planet. Sci. Lett.* **402**, 99–106 (2014).

34. Liu, K. H., Gao, S.S., Silver, P.G., & Zhang, Y.K. Mantle layering across central South America. *J. Geophys. Res.* **108**, 2510 (2003).

SECTION

2. CONCLUSIONS

We imaged the MTZ discontinuities beneath Iceland using P-to-S receiver functions. The central and eastern parts of Iceland (the central zone) are characterized by a normal to slightly thicker-than-normal MTZ, while the peripheral area demonstrates a thinner-than-normal MTZ. We discussed several possible models to interpret the results based on recently published geodynamic and mineralogical studies. The MTZ thickness and the apparent topography of the d410 and the d660 are controlled by velocity anomaly, thermal anomaly, and the associated mineral phase transitions. The P wave velocity (temperature) anomalies caused by the plume are estimated to be ranged from -0.95 % (178 K) at the peripheral area to -1.16% (218 K) at the central zone. The Clapeyron slope is increasing concomitant with increasing proportions of garnet phase toward the plume center. The phase transitions at the d660 beneath Central Iceland has a significant impact on the plume dynamics. The increasing proportion of garnet phase with increasing temperature significantly promotes the plume upwelling. The proposed broad plume model from this study is consistent with recently published geodynamic model.

VITA

Dan Wang was born in Henan Province, China. He was transferred to Missouri S&T in 2011 as one of the earliest transfer students from the '2+2' program between S&T and universities in China. He received his undergraduate degrees in geology and geophysics from both China University of Petroleum (East China) and Missouri S&T. In 2012, he served as the vice president of the Chinese Students and Scholars Association (CSSA) and received the Undergraduate Student Award in recognition of his outstanding service around campus. In 2018, he was elected as the president of the Society of Exploration Geophysicists (SEG) Missouri S&T Student Chapter and received the SEG/Chevron Student Leadership Award. He has a wide range of teaching and research experience, including geophysics, geochemistry, physical geology, and engineering geology. He received his Ph.D. degree in Geology and Geophysics from Missouri S&T in May of 2020 under the supervision of Dr. Stephen S. Gao. He also received a graduate certificate in Business Intelligence from the Department of Business and Information Technology in May 2020.